The human methyltransferase ZCCHC4 catalyses N^6-methyladenosine modification of 28S ribosomal RNA

Rita Pinto[1], Cathrine B. Vågbø[2,3], Magnus E. Jakobsson[4], Yeji Kim[5,6], Marijke P. Baltissen[7], Marie-Françoise O'Donohue[8], Ulises H. Guzmán[4], Jędrzej M. Małecki [1], Jie Wu[5,6], Finn Kirpekar[9], Jesper V. Olsen[4], Pierre-Emmanuel Gleizes[8], Michiel Vermeulen[7], Sebastian A. Leidel [5,6], Geir Slupphaug[2,3] and Pål Ø. Falnes [1,*]

[1]Department of Biosciences, Faculty of Mathematics and Natural Sciences, University of Oslo, Oslo 0316, Norway, [2]Department of Clinical and Molecular Medicine, Norwegian University of Science and Technology, NTNU, NO-7491 Trondheim, Norway, [3]Proteomics and Modomics Experimental Core (PROMEC), NTNU and the Central Norway Regional Health Authority, NO-7491 Trondheim, Norway, [4]Proteomics Program, Faculty of Health and Medical Sciences, Novo Nordisk Foundation Center for Protein Research (NNF-CPR), University of Copenhagen, Blegdamsvej 3B, 2200 Copenhagen, Denmark, [5]Max Planck Research Group for RNA Biology, Max Planck Institute for Molecular Biomedicine, 48149 Muenster, Germany, [6]Department of Chemistry and Biochemistry, University of Bern, 3012 Bern, Switzerland, [7]Department of Molecular Biology, Faculty of Science, Radboud Institute for Molecular Life Sciences, Oncode Institute, Radboud University Nijmegen, Nijmegen 6500 HB, The Netherlands, [8]Laboratoire de Biologie Moléculaire Eucaryote, Centre de Biologie Intégrative, Université de Toulouse, CNRS, UPS, Toulouse, France and [9]Department of Biochemistry and Molecular Biology, University of Southern Denmark, Campusvej 55, 5230 Odense M, Denmark

ABSTRACT

RNA methylations are essential both for RNA structure and function, and are introduced by a number of distinct methyltransferases (MTases). In recent years, N^6-methyladenosine (m^{6}A) modification of eukaryotic mRNA has been subject to intense studies, and it has been demonstrated that m^{6}A is a reversible modification that regulates several aspects of mRNA function. However, m^{6}A is also found in other RNAs, such as mammalian 18S and 28S ribosomal RNAs (rRNAs), but the responsible MTases have remained elusive. 28S rRNA carries a single m^{6}A modification, found at position A4220 (alternatively referred to as A4190) within a stem–loop structure, and here we show that the MTase ZCCHC4 is the enzyme responsible for introducing this modification. Accordingly, we found that ZCCHC4 localises to nucleoli, the site of ribosome assembly, and that proteins involved in RNA metabolism are overrepresented in the ZCCHC4 interactome. Interestingly, the absence of m^{6}A4220 perturbs codon-specific translation dynamics and shifts gene expression at the translational level. In summary, we establish ZCCHC4 as the enzyme responsible for m^{6}A modification of human 28S rRNA, and demonstrate its functional significance in mRNA translation.

INTRODUCTION

The RNAs within a cell contain a wide range of small enzyme-mediated modifications, which contribute to expanding the repertoire of RNA building blocks (1). These modifications, collectively, are instrumental for mediating appropriate RNA folding, maintaining RNA structure and enabling the various RNA functions. More than 100 different RNA modifications have been described, and all RNA species carry modifications, with tRNAs being most heavily modified (2). Methylation is the most common type of RNA modification, and numerous different methylated nucleosides are present in RNA (3).

It was discovered several decades ago that the modification N^6-methyladenosine (m^{6}A) is abundant in eukaryotic mRNAs (4,5). These initial findings were followed by the identification of the catalytically active component of the corresponding human methyltransferase (MTase) as

METTL3 (aka MT-A70) ([6]). Also, a regulatory function for the m^{6}A modification was suggested by the observation that sporulation was accompanied by increased m^{6}A levels in the budding yeast *Saccharomyces cerevisiae* ([7]). In recent years, substantial progress has been made regarding m^{6}A modification and its functional significance. Methods were developed to assess m^{6}A modification transcriptome-wide ([8,9]), and numerous proteins have been uncovered that are responsible for introducing, recognizing and removing m^{6}A, referred to as writers, readers, and erasers, respectively ([10]). Moreover, it has also been demonstrated that m^{6}A modification plays an important role in regulating and optimizing many aspects of RNA function and biogenesis, including splicing, nuclear export, translation and turnover ([11–14]).

So far, three human MTases that install m^{6}A in RNA have been discovered. The majority of m^{6}A in mRNA is introduced by the MTase METTL3, which is found in complex with several additional proteins required for methylation, including the related protein METTL14 ([15–17]). The METTL3 complex installs m^{6}A at specific RRACH consensus sequences (R = A, G; H = A, C, U), but mRNA is also modified at non-RRACH sites. METTL16 was recently discovered as a novel MTase that introduces m^{6}A in a stem–loop structure in the U6 spliceosomal RNA, but also modifies similar structures in various mRNAs, thereby regulating their function ([18,19]). Finally, a 2′-O-ribose methylated form of m^{6}A (m^{6}Am) is installed as part of the cap structure in mRNAs whose first transcribed nucleotide is an adenosine, and two very recent studies identified PCIF as the long-sought MTase responsible for N^6-methyladenosine formation at the cap ([20,21]).

In humans, five proteins of the YTHD family, which all contain a so-called YTH domain, are the primary reader proteins responsible for recognising m^{6}A modifications in mRNA. The closely related YTHDF1, YTHDF2 and YTHDF3 are localized to the cytosol where they promote translation and turnover of m^{6}A containing mRNAs ([12,13,22,23]). The nuclear reader YTHDC1 regulates splicing and export of m^{6}A containing mRNAs ([11,14]). YTHDC2, found both in the cytosol and the nucleus, interacts with the ribosome, where it promotes efficient translation of its target mRNAs, while also enhancing their degradation ([24,25]). Finally, the two oxidative demethylases ALKBH5 and FTO are erasers responsible for removal of m^{6}A, thus contributing to the dynamic nature of this modification ([26,27]).

The ribosome represents a universally conserved molecular machine that mediates the essential function of translating genetic information, in the form of mRNA, into protein sequence. The human ribosome contains four RNAs and 80 proteins, distributed between a small (40S) and a large (60S) subunit ([28]). The two largest rRNAs are the 18S rRNA (1869 nucleotides) and 28S rRNA (5035 nucleotides), which are the found in the 40S and 60S subunits, respectively ([29]). 18S and 28S rRNA both contain numerous posttranscriptional modifications, the majority being pseudouridines and 2′-O-ribose methylations ([29,30]). These are introduced by ribonucleoprotein (RNP) complexes containing snoRNAs that guide the relevant enzymatic machineries to specific locations in the RNA sequence ([31]).

Additionally, several snoRNA-independent 'stand-alone' enzymes introduce various rRNA modifications, primarily methylations ([32,33]). The assembly and maturation of the ribosome, occurring primarily within nucleoli, is a highly orchestrated process where the timely insertion of specific modifications is essential ([34]). Here, snoRNA-directed introduction of pseudouridine and methylribose occurs at relatively early stages of ribosome maturation, whereas snoRNA-independent modifications are believed to occur at later stages ([34]). The snoRNA-independent modifications include a single instance of m^{6}A in each of 18S and the 28S rRNAs ([29]). However, as the MTases responsible for m^{6}A modification of rRNA have remained elusive, it has been difficult to investigate the functional significance of these modifications.

Bioinformatics analysis indicates that the human genome encodes ∼200 different MTases that use the methyl donor *S*-adenosylmethionine (AdoMet) ([35]). The function of a large proportion of these enzymes remains elusive, though we have unravelled the function of several orphan MTases in recent years. In particular, we have identified several MTases that target lysines in proteins, but also RNA-specific MTases (see e.g. ([36–42])). Here, we have explored the function of the human orphan MTase ZCCHC4. We found that proteins involved in RNA metabolism were over-represented in the ZCCHC4 interactome, and that ZCCHC4 was localised to nucleoli, where ribosome assembly occurs. In agreement with this, we found that ablation of ZCCHC4 caused a strong reduction of m^{6}A in total rRNA, and that this was due to a complete abolishment of the single m^{6}A modification in 28S rRNA. The absence of m^{6}A formation on 28S rRNA leads to ribosomes with altered activity as indicated by codon-specific translation defects. In conclusion, we here establish ZCCHC4 as a novel MTase responsible for introducing m^{6}A at position 4220 in 28S rRNA.

MATERIALS AND METHODS

Bioinformatics analysis

Protein sequences were aligned using the MAFFT algorithm embedded in JalView ([43,44]). Three-dimensional structures were visualized using The PyMOL Molecular Graphics System (Schrodinger).

Gene cloning and mutagenesis

The open reading frames (ORFs) for human ZCCHC4 and RPL3 were amplified from U87-MG and HeLa cDNA, respectively, using Phusion DNA Polymerase HF (Thermo Fisher Scientific) and primers that generated PCR products with target vector-specific overhangs. Cloning into the vectors by homologous recombination was then performed using In-Fusion HD Cloning (Clontech) according to the manufacturer's instructions.

Briefly, to generate ZCCHC4 with a C-terminal 6× His-tag, the ORF was cloned into the pET28a expression vector (Novagen), between NcoI and XhoI sites. To generate the pcDNA5/FRT/TO-ZCCHC4-GFP and pcDNA5/FRT/TO-RPL3-GFP constructs, ZCCHC4 or

RPL3 ORFs, respectively, were first fused with green fluorescent protein (GFP)-codon optimized ORF derived from the pEGFP-N1 vector and then the fragments were subcloned into pcDNA5/FRT/TO (Invitrogen) using KpnI and NotI. A fragment encoding GFP only was cloned into pcDNA5/FRT/TO between KpnI and NotI, using standard ligation-dependent cloning, generating the pcDNA5/FRT/TO-GFP construct. Finally, pMRFP-RPL3 construct was made by cloning the RPL3 ORF into pMRFP-C1 vector using SacI and SacII.

Site-directed mutagenesis for correction of the ZCCHC4 ORF from U87-MG cells and mutation of His-tagged ZCCHC4 (D276A-mutated ZCCHC4) was performed using the QuikChange II site-directed mutagenesis kit (Stratagene) according to the manufacturer's instructions. All constructs were sequence-verified, including tags. All primers used for cloning are listed in Supplementary Table S1.

Cell culture and generation of stable cell lines

Cell lines for doxycycline (Dox) inducible overexpression of GFP, GFP-tagged ZCCHC4 or RPL3 were generated using the Flp-In™ T-REx™-293 system (Invitrogen) according to the manufacturer's instructions. Briefly, Flp-In T-REx HEK-293 cells were cotransfected with pOG44 and pcDNA5/FRT/TO-ZCCHC4-GFP, pcDNA5/FRT/TO-Rpl3-GFP or pcDNA5/FRT/TO-GFP using Fugene6 (Roche). Clones that successfully integrated the constructs were selected with 200 μg/ml hygromycin B (Invitrogen). Cells were thereafter maintained in high-glucose DMEM (Gibco) supplemented with 10% (v/v) FBS (Gibco), 100 U/ml streptomycin (Invitrogen), and 100 U/ml penicillin (Lonza). In order to induce ZCCHC4-GFP, RPL3-GFP or GFP, 1 μg/ml of Dox was added to the culture media for 24 or 48 h.

ZCCHC4-deficient human haploid HAP-1 cells were generated as a custom (non-exclusive) project with Horizon Genomics (Austria). *ZCCHC4* knock-out (KO) was achieved by 19 bp deletion on exon 7, generating a premature STOP codon. Both HAP-1 'wild-type' (WT) and HAP-1 *ZCCHC4* KO cells were maintained in high-glucose IMDM (Gibco) supplemented with 10% (v/v) FBS (Gibco), 100 U/ml streptomycin (Invitrogen), and 100 U/ml penicillin (Lonza).

Zcchc4 KO mouse K:Molv NIH/3T3 fibroblasts and J1 embryonic stem (ES) cells were obtained by CRISPR/Cas9 genome editing using a plasmid coding for a high fidelity Cas9 protein (VP12), a BPK1520 (Addgene)-derived plasmid where suitable guide RNAs (gRNA) were cloned into, and a construct coding for the neomycin resistance gene flanked by ∼900 bp of homology arms to allow for homologous recombination into the *Zcchc4* gene. All primers used for cloning of homology arms are listed in Supplementary Table S1. Lipofectamine 3000 (Invitrogen) was used as transfection agent according to the manufacturer's instructions. gRNA sequence (GACATTTCTGTCGCCCAGCT) targeting *Zcchc4* exon 4 were designed using the optimized CRISPR design online tool (http://crispr.mit.edu/) provided by the Zhang laboratory at the Massachusetts Institute of Technology, Boston.

K:Molv NIH/3T3 and J1 transfected cells were selected with 200 or 300 μg/ml G418 (Gibco), respectively, and *Zcchc4* KO targeted region of selected clones was then sequence-verified. The primers used for sequencing are listed in Supplemental Table 1. One clone where both *Zcchc4* alleles have been disrupted was chosen for each cell line. Sequencing of the CRISPR/Cas9 target region revealed that one of the alleles was disrupted by neomycin resistance gene insertion in both cell lines, whereas the other allele was mutated generating a shift in *Zcchc4* ORF (178bp deletion in J1 and 5bp deletion in K:Molv NIH/3T3 cells).

Both WT and *Zcchc4* KO J1 cells were maintained in DMEM (Gibco) supplemented with 15% (v/v) FBS (Gibco), 1% L-glutamine (Gibco), 100 U/ml streptomycin (Invitrogen), 100 U/ml penicillin (Lonza), 1% non-essential amino acids (Gibco), 60 μM β-mercaptoethanol (Gibco) and leukemia inhibitory factor (LIF). J1 *Zcchc4* KO cells were also maintained in the presence of 200 μg/ml G418 (Gibco). Both WT and *Zcchc4* KO K:Molv NIH/3T3 cells were maintained in high-glucose DMEM (Gibco) supplemented with 10% (v/v) FBS (Gibco), 100 U/ml streptomycin (Invitrogen), and 100 U/ml penicillin (Lonza). K:Molv NIH/3T3 *Zcchc4* KO cells were also maintained in the presence of 300 μg/ml G418 (Invitrogen).

Transient transfection and fluorescence microscopy

After 24 h induction of ZCCHC4-GFP fusion protein expression in Flp-In T-REx HEK-293 using Dox, cells were transfected with the pMRFP-RPL3 plasmid using Lipofectamine 3000 (Invitrogen) as transfection agent according to the manufacturer's instructions. 24 h after transfection, cells were fixed in cold acetone for 10 min and incubated with 1 μg/ml Hoechst 33258 (Sigma-Aldrich) for nuclear counterstaining. Cell staining was then analyzed using an Olympus FluoView 1000 (IX81) confocal fluorescence microscopy system with a PlanApo 60× NA 1.1 oil objective (Olympus). The fluorophores were excited at 405 nm (Hoechst 33258), 488 nm (GFP) and 559 nm (RFP). A Kalman filter was used to record multi-channel images.

GFP immunoprecipitation (IP)

Flp-In T-REx HEK-293 cells where ZCCHC4-GFP, RPL3-GFP and GFP expression had been induced using Dox for 48 h were lysed for 15 min at 4°C in RIPA buffer (Sigma) supplemented with 1 mM phenylmethylsulfonyl fluoride (PMSF) (Sigma) in the presence of cOmplete™ EDTA-free protease inhibitor cocktail (Roche). The cleared lysate was then diluted in a buffer containing 50 mM Tris–HCl, pH 7.5, 150 mM NaCl and 0.5 mM EDTA and GFP IP was performed using GFP-Trap® agarose beads (Chromotek) for 2 h at 4°C. After washing the beads with the dilution buffer, samples were further processed for mass spectrometry analysis.

MS identification of proteins interacting with GFP-fusion proteins

Proteins from GFP pulldown experiments were essentially processed and analyzed as previously described (37). In

brief, proteins enriched by GFP-Trap beads were eluted and digested by adding 25 µl 2M urea, 1 mM DTT and 5 ng/µl trypsin. The resulting peptides were alkylated by adding 5 mM iodoacetamide and then desalted using StageTips (45). Desalted peptides were analyzed using an EASY-nLC 1200 system connected to a QExactive HF mass spectrometer (Thermo Fisher Scientific) operated in a data dependent acquisition mode (46). Label-free quantification of proteins from pull-down experiment was performed using the MaxLFQ algorithm (47) embedded in the MaxQuant package (48).

Total RNA extraction and isolation of RNA species

Total RNA was extracted using TRI Reagent (Sigma). Large (>∼200 nt) and small (<∼200 nt) fractions of RNA were isolated using the mirVana miRNA Isolation Kit (Thermo Fisher Scientific) as recommended by the manufacturer. Poly-A-RNA enrichment from total RNA was performed using magnetic beads Oligo-d(T)25 (NEB) in the presence of lithium dodecyl sulfate and lithium chloride. For each 10 µg of total RNA, 100 µl of the beads were used. For northern blot analyses, following TRI reagent extraction, the aqueous phase was further extracted with phenol–chloroform–isoamyl alcohol (25:24:1; Sigma), then with chloroform. Total RNAs were recovered after precipitation with 2-propanol and then rinsed twice in 70% ethanol.

RNA analysis by northern blot

Total RNAs were denatured for 10 min at 70°C and separated on a 1.2% agarose gel containing 1.2% formaldehyde and 1× Tri/Tri buffer (30 mM triethanolamine, 30 mM tricine, pH 7.9) (3 µg RNAs/lane). Smaller RNAs were separated on 6% polyacrylamide gels (acrylamide:bisacrylamide 19:1) in Tris-borate EDTA buffer containing 7 M urea and electrotransferred to a nylon membrane. RNAs were transferred to a Hybond N$^+$ nylon membrane (GE Healthcare) by passive transfer. Prehybridization was performed for 1 h at 45°C in 6× SSC, 5× Denhardt's solution, 0.5% SDS, 0.9 µg/ml tRNA. The 5′-radiolabeled oligonucleotide probes were incubated overnight. The sequences of the probes are indicated in Supplementary Table S2. Membranes were washed twice for 10 min in 2× SSC, 0.1% SDS and once in 1× SSC, 0.1% SDS, and then exposed. Signals were acquired with a Typhoon Trio PhosphoImager (GE Healthcare) and quantified using the MultiGauge software.

Quantification of RNA modifications using LC-MS/MS

RNA was hydrolyzed to ribonucleosides by 20 U benzonase (Santa Cruz Biotech) and 0.2 U nuclease P1 (Sigma) in 10 mM ammonium acetate pH 6.0 and 1 mM magnesium chloride at 40°C for 45 min, then added ammonium bicarbonate to 50 mM, 0.002 U phoshodiesterase I and 0.1 U alkaline phosphatase (Sigma) and incubated further at 37°C for 45 min. The hydrolysates were added 3 volumes of acetonitrile and centrifuged (16 000 g, 30 min, 4°C). The supernatants were dried and dissolved in 50 µl water for LC-

MS/MS analysis of modified and unmodified ribonucleosides. Chromatographic separation was performed using an Agilent 1290 Infinity II UHPLC system with an ZORBAX RRHD Eclipse Plus C18 150 × 2.1 mm ID (1.8 µm) column protected with a ZORBAX RRHD Eclipse Plus C18 5 × 2.1 mm ID (1.8 µm) guard column (Agilent). The mobile phase consisted of water and methanol (both added 0.1% formic acid) run at 0.23 ml/min, for modifications starting with 5% methanol for 0.5 min, followed by a 2 min gradient of 5–15% methanol, a 4 min gradient of 15–95% methanol and 4 min re-equilibration with 5% methanol. A portion of each sample was diluted for the analysis of unmodified ribonucleosides and was chromatographed isocratically with 20% methanol. Mass spectrometric detection was performed using an Agilent 6495 Triple Quadrupole system operating in positive electrospray ionization mode, monitoring the mass transitions 282.1/150.1 (m^{6}A, m^{1}A), 296.1/164.1 (m$^6_2$A), 282.1/136.1 (Am), 268.1/136.1 (A), 244.1/112.1 (C), 284.1/152.1 (G), 245.1/113.1 (U).

MALDI mass spectrometry/tandem mass spectrometry

Total RNA was hybridized to a DNA oligodeoxynucleotide complementary to position 4201–4250 of human 28S rRNA, followed by digestion with mung bean nuclease and RNase A as described previously (49). The desired 28S rRNA sub-fragment was purified by polyacrylamide gel electrophoresis and digested with RNase T1 for analysis on a Bruker UltraFlex MALDI mass spectrometer (50). 1–2 pmol rRNA sub-fragment were RNase digested to completion and analysed directly using 3-hydroxypicolinic acid as matrix. The observed masses were compared to theoretical masses calculated using GPMAW software (Lighthouse Data, Denmark). Tandem mass spectrometry to confirm the exact position of the observed modification was performed on a Waters Q-TOF MALDI Premiere instrument (Waters, Manchester, UK) in positive ion mode as previously described (51).

Expression and purification of recombinant His-tagged ZC-CHC4

Constructs encoding His-tagged wild-type (WT) or D276A mutated ZCCHC4 were transformed into the *Escherichia coli* BL21-(DE3)-RIPL strain (Agilent Technologies), and protein expression was induced with 0.1 mM IPTG, at 18°C, overnight. Bacteria were harvested by centrifugation, lysed in Lysis Buffer (50 mM Tris–HCl pH 7.4, 100 mM NaCl, 1% Triton X-100, 5% glycerol, 20 mM imidazole, 1× cOmplete (EDTA-free) protease inhibitor cocktail (Roche), 10 U/ml Benzonase nuclease (Sigma-Aldrich)) and lysates clarified by centrifugation (45 000 × g, 30 min). Cleared lysates were applied to Ni-NTA-agarose (Qiagen) equilibrated in Lysis Buffer. The resin was washed sequentially with Wash Buffer (50 mM Tris–HCl pH 7.4, 5% glycerol, 20 mM imidazole) supplemented with 0.5 M NaCl, then with Wash Buffer supplemented with 2.0 M NaCl, and finally again with Wash Buffer supplemented with 0.5 M NaCl. His-tagged proteins were eluted using Wash Buffer supplemented with 0.5 M NaCl and 200 mM imidazole, and buffer-exchanged to Storage Buffer (50 mM Tris–HCl pH 8.0, 100 mM NaCl,

10% glycerol) using centrifugal concentrators (Sartorius, 50 kDa cut-off). Proteins were aliquoted and stored at −20°C. Proteins were ∼50% pure as assessed by SDS-PAGE and Coomassie Blue staining. Protein concentration was determined using Pierce BCA Protein Assay Kit (Thermo Fisher Scientific).

In vitro methyltransferase assay using [³H]AdoMet

To test MTase activity of ZCCHC4, 10 μL reactions were assembled on ice containing: 1× MTase Assay Buffer (50 mM Tris–HCl pH 8.0, 5 mM $MgCl_2$, 1 mM DTT), 0.5 μCi of [³H]AdoMet (Perkin-Elmer) ([AdoMet]$_{total}$ = 0.64 μM, specific activity = 78.2 Ci/mmol), 2 μg of recombinant ZCCHC4 (WT or D276A-mutated), and 2 μg of HPLC-purified biotinylated RNA oligonucleotides (Midland Certified Reagent Company, Texas, USA), either unmethylated (5′-(Biotin)AUCACCUGUCAAACGGUAAC GCAGGUG-3′), or methylated (5′-(Biotin)AUCACCUG UCAAACGGUA(N^6-methyl-rA)CGCAGGUG-3′). Reactions were incubated for 90 min at 28°C. After that, test samples were treated with proteinase K (Qiagen, 100× diluted) and incubated for another 30 min at 28°C, while control samples were analyzed by SDS-PAGE and Coomassie staining, to verify equal protein loading. Biotinylated RNA oligonucleotides in test samples were recovered by binding to Dynabeads M280 Streptavidin (Thermo Fisher Scientific) equilibrated in B&W Buffer (50 mM Tris–HCl pH 7.4, 0.5 mM EDTA, 1 M NaCl), according to the manufacturer's instructions. Dynabeads with bound oligonucleotides were washed three times with B&W Buffer, resuspended in 200 μl of 0.1 M KOH, and transferred to scintillation vials filled with 4 ml of Ultima Gold scintillation liquid (Perkin-Elmer). The incorporated radioactivity was measured in 1900 TR liquid scintillation analyzer (Packard). The experiment was performed two times, in triplicates. All data points were included in the statistical analysis.

Identification of proteins interacting with the A4220-m⁶A stem–loop

For cell lysis, trypsinized HeLa cells were first washed extensively with PBS. Cells were then resuspended and lysed by adding five pellet volumes of whole cell extraction buffer (50 mM Tris–HCl, pH 8, 150 mM NaCl, 1% NP-40, 0.5 mM DTT, 10% glycerol and EDTA-free cOmplete™ protease inhibitor cocktail (Roche). This suspension was then incubated at 4°C for 90 min in a rotation wheel, followed by a 30 min centrifugation at 21 000 g at 4°C. Soluble whole cell extracts were then snap-frozen in liquid nitrogen until further usage.

The dimethyl RNA pulldowns and mass spectrometry analysis were performed as follows: Buffer solutions were prepared with high-quality, RNase-free reagents. Four individual pull-downs were performed for each dimethyl-based RNA pulldown experiment. 20 μl of a 50% slurry of streptavidin Sepharose high-performance beads (GE Healthcare) were used for each pull-down. Beads were first washed twice with 1 ml of RNA binding buffer (50 mM HEPES–HCl, pH

7.5, 150 mM NaCl, 0.5% NP40 (v/v), 10 mM $MgCl_2$). Samples were centrifuged in a table top centrifuge for 3 min at 1500 × g at 4°C after each wash step. Beads were incubated with the RNase inhibitor RNasin plus (Promega) in RNA binding buffer (100 μl buffer with 0.8 units of RNasin/μl) for 15 min at 4°C in a rotating wheel to remove and inactivate RNases. Beads were then centrifuged and RNasin– RNase complexes were removed. Yeast tRNA (50 μg/ml; AM7119; Life Technologies) in RNA binding buffer was added to preblock the beads. After overnight incubation at 4°C in a rotation wheel the beads were washed twice with RNA binding buffer followed by incubation with 5 μg of the biotinylated RNA probe in a total volume of 600 μl RNA binding buffer. Biotinylated probes were allowed to bind to the streptavidin beads for 30 min at 4°C in a rotation wheel. Beads were then washed with 1 ml of RNA wash buffer (50 mM HEPES–HCl, pH 7.5, 250 mM NaCl, 0.5% NP40 and 10 mM $MgCl_2$) followed by two washes with protein incubation buffer (10 mM Tris–HCl, pH 7.5, 150 mM KCl, 1.5 mM $MgCl_2$, 0.1% (v/v) NP40, 0.5 mM DTT and cOmplete™ EDTA-free protease inhibitor mixture (Roche). Beads were subsequently incubated with 1 mg of whole cell extract for 30 min at room temperature followed by 90 min at 4°C in a rotation wheel, in a total volume of 600 μl protein incubation buffer supplemented with 30 μg yeast tRNA and 200 units RNasin. The beads were then washed three times with 1 ml protein incubation buffer followed by two washes with PBS.

Next, beads were resuspended in 50 μl elution buffer (50 mM Tris, pH 8.5, 2 M urea and 10 mM DTT) and incubated for 20 min at room temperature in a thermoshaker at 1500 rpm. Iodoacetamide was then added to a final concentration of 55 mM, and beads were incubated in a thermoshaker for 10 min shaking at 1500 rpm in the dark. 250 ng of trypsin was added for 2 h at room temperature in a thermoshaker to partially digest bead-bound proteins. The supernatant was then collected in a separate tube and 50 μl of fresh elution buffer was added to the beads for 5 min at room temperature in a thermoshaker. Both eluates were pooled and 100 ng of fresh trypsin was added for overnight digestion of the proteins at room temperature.

The resulting tryptic peptides were desalted using C18 Stage tips (52) and differentially labeled with dimethyl isotopes CH_2O or CD_2O (53). Labeled peptides were mixed to create forward and reverse reactions [forward reaction: control probe, CH_2O (light), N^6-methyl-rA probe, CD_2O (heavy); reverse reaction: N^6-methyl-rA probe, CH_2O (light), control probe, CD_2O (heavy)]. Samples were measured by LC–MS on an Orbitrap-Fusion-Tribrid instrument and raw mass spectrometry data was analyzed by MaxQuant (48) and visualized essentially as described (54).

Ribosome profiling

Ribosome profiling libraries of ZCCHC4-deficient HAP-1 cells were generated in triplicates and WT HAP-1 cells were generated in duplicates. Medium was aspirated, cells were washed with ice-cold PBS and flash frozen in liquid nitrogen. Subsequently, the dish was transferred to ice, 400

μl lysis buffer [10 mM Tris–HCl pH 7.5, 100 mM NaCl, 5 mM $MgCl_2$, 1% Triton X-100, 0.5 mM DTT, 0.5% deoxycholate (w/v) and 100 μg/ml cycloheximide (CHX)] was dripped onto the cells and cells were scraped after lysis buffer had thawed. Next, samples were centrifuged for 5 min at 4°C and 10 000 × g. Ribosome protected fragments were generated by digesting 10 A_{260} units of the cleared lysate with 900 U RNase I (ThermoFisher) at 22°C. The reaction was stopped after 1 h by addition of 15 μl Superase In (ThermoFisher) and loaded on a 10–50% (w/v) sucrose gradient in 50 mM Tris-HCl pH 7.5, 50 mM NH_4Cl, 12 mM $MgCl_2$, 0.5 mM DTT, 100 μg/ml CHX and centrifuged for 3 h at 35 000 rpm and 4°C in a TH-641 rotor (Thermo Scientific). Monosomes were fractionated and total RNA isolated. Subsequently, RNA was separated on 15% polyacrylamide gels (8 M urea, 1× TBE buffer) and 28–32 nt ribosome footprints were extracted from the gel. Finally, libraries were generated as described (55) but using adenylated 3′-adapters that contained four randomized nucleotides to reduce ligation biases (56). Libraries were mapped to the hg38 transcriptome (UCSC_knownGene) and subsequent analysis was performed using a custom script. A-site codon occupancy was determined as previously described (57), while excluding the first 15 nt of each ORF to reduce position-specific biases. 29–31 nt long reads starting in the 0-frame were used and the A-site defined as positions 15–17 from the start of the read. A-site occupancy was normalized to the adjacent codons in the +1, +2 and +3 positions. Ribosome occupancy at the +1 position (18–20 nt from the start of the read), was normalized to occupancy at the +2, +3 and +4 positions.

DESeq2 using a Padjusted threshold of 0.05 and a $\log_2$ fold change threshold of 0.5 was used for differential gene translation analysis of ribosome protected fragments (58). Gene ontology (GO) term analysis was performed using GOrilla (59).

Proteomic characterization of polysomes

For mass spectrometry sample preparation, the polysome containing fractions were diluted 2× in 6 M guanidinium chloride, 75 mM NaCl, 100 mM Tris–HCl, pH 8.5, 5 mM tris(2-carboxyethyl)phosphine (TCEP), 10 mM chloroacetamide (CAA) and sequentially digested with Lys-C and trypsin. The resulting peptides were desalted on C18 Sep-Pak (Waters) columns. The eluates from Sep-Pak columns were reconstituted in 0.1% trifluoroacetic acid and 5% acetonitrile. All samples were analyzed using a Q-Exactive HF mass spectrometer connected to an EASY-nLC (Thermo Fisher Scientific). Peptides were chromatographically separated on a 15 cm long column, 75-μm inner diameter, packed in-house with 1.9 μm C18 beads (Reprosil-Pur AQ, Dr Maisch) using a 60 min gradient. The mass spectrometer was operated in a data-dependent acquisition mode using a top-6 method. The resolution for full scans was set to 60 000 and peptides dissociated using HCD were analyzed at a 30,000 resolution. All raw mass spectrometry output files were analyzed using MaxQuant (version 1.6.6.0) and subsequent statistical analysis was carried out using Perseus (version 1.6.5.0).

RESULTS

ZCCHC4 —domain architecture, evolutionary distribution and key motifs

Bioinformatics analysis indicated that the uncharacterized human protein ZCCHC4, which carries CCHC zinc finger (Pfam PF00098), also contains a MTase domain, which belongs to the seven β-strand (7BS, also referred to as 'Rossmann-fold') class of MTases (35). The MTase domain is found in the middle portion of ZCCHC4, flanked by N- and C-terminal regions that are rich in Cys and His residues (Figure 1A). The C-terminal region contains the classic CCHC zinc finger, as well as several additional non-canonical CCHC zinc fingers (see below), while the Cys/His-rich N-terminal part lacks annotated motifs (Figure 1A). Putative ZCCHC4 orthologues are present in a wide range of animals, and sequence alignments reveal several interesting conserved motifs (Figure 1B, C).

First, ZCCHC4 contains a highly conserved DPPF motif within its MTase domain (Figure 1A, B). Such a motif, with consensus sequence (S/N/D)PP(Y/F/W) has previously been shown to be characteristic and essential for several MTases that target nucleic acid substrates (60). Moreover, an Asp (D) residue in the first position of this motif, as is the case for ZCCHC4, is typical of MTases that introduce m^6A, such as human METTL3/METTL14 (61). The human MTase that is most similar to ZCCHC4 also carries a conserved DPP(F/Y) motif, and this MTase was initially denoted 'N^6-adenine specific MTase 2' (gene: N6AMT2). However, this enzyme was established as a lysine-specific protein MTase (62), suggesting that the target of ZCCHC4 cannot be readily predicted from sequence and structural features.

Second, the C-terminal region of ZCCHC4 contains a number of conserved Cys and His residues (Fig 1C). The classic CCHC-type zinc finger (consensus $C-X_2-C-X_4-H-X_4-C$) is found at the end of this region. In addition, the C-terminal region contains several repetitions of the motif $C-X_2-C-X_n-HC$ (where n is variable), thus showing similarity to the so-called DHHC-motif found in palmitoyltransferases, as well as to a similar domain in the ubiquitin ligase RCHY1 (PIRH2) (63,64). Notably, the three-dimensional structures of the corresponding regions in RCHY1 and in the palmitoyltransferase DHHC20 have demonstrated a distinct organization, where several partially overlapping (in the primary sequence), non-canonical CCHC zinc fingers each coordinate a zinc ion (63,65) (Figure 1D). From the near-perfect alignment of Cys and His residues between RCHY1, DHHC20 and ZCCHC4 (Figure 1D), one may infer that the corresponding region in ZCCHC4 putatively contains four non-canonical CCHC zinc fingers, binding four zinc atoms (Figure 1C). In conclusion, this initial bioinformatics analysis indicates that human ZCCHC4 is a zinc binding MTase, with a possible role in introducing m^6A into nucleic acid substrates.

ZCCHC4 is localized to nucleoli

To elucidate ZCCHC4 function, we set out to investigate its subcellular localisation by using a ZCCHC4-GFP fusion protein. To this end, we generated a human cell line
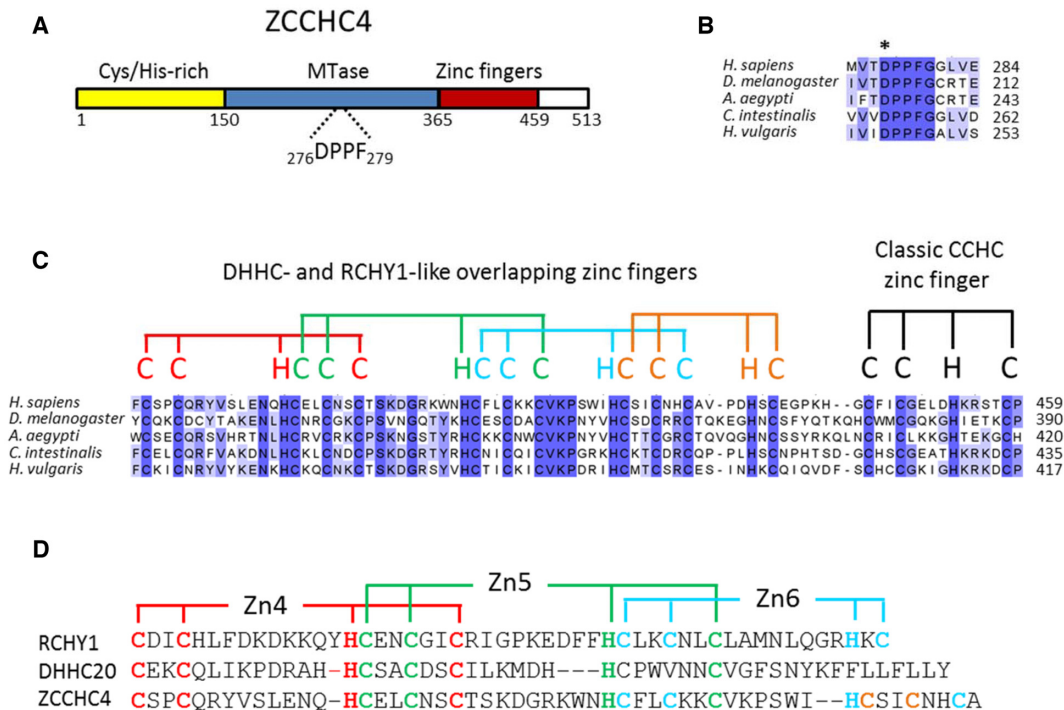
Figure 1. Domain architecture and sequence motifs of ZCCHC4. (**A**) ZCCHC4 domain architecture. ZCCHC4 consists of an N-terminal region rich in conserved histidine and cysteine residues (yellow), a middle MTase domain (blue) containing a conserved DPPF motif (see also (**B**)), and a C-terminal domain (red) containing five putative zinc fingers (see also (C, D)). (**B**) ZCCHC4 contains a conserved DPPF motif within its MTase domain. Shown is part of a sequence alignment of putative ZCCHC4 orthologues from *Homo sapiens* (Q9H5U6.3), *Drosophila melanogaster* (NP_610973.3), *Aedes aegypti* (XP_001649112.1), *Ciona intestinalis* (XP_002124158.1), *Hydra vulgaris* (XP_002158966.1). The asterisk indicates the conserved Asp residue that was mutated in human ZCCHC4 to make a putatively inactive mutant (D276A). (**C**) Conserved cysteines and histidines within the C-terminal domain of ZCCHC4 constitute canonical and non-canonical CCHC zinc fingers. Shown is an alignment of the C-terminal domain of ZCCHC4 from various animals. In black is indicated the classic CCHC zinc finger (consensus $C-X_2-C-X_4-H-X_4-C$, X is any amino acid), and in red, green, blue and orange are shown putative overlapping non-canonical CCHC zinc fingers. The putative existence of these zinc fingers was inferred from the reported zinc coordination in the structures of the RCHY1 and DHHC20 proteins (see D). (**D**) Alignment of ZCCHC4 with non-canonical CCHC4 zinc fingers of RCHY1 (Q96PM5.1) and DHHC20 (Q5W0Z9). The three shown CCHC4 zinc fingers of RCHY1 (shown in red, green and blue) were previously shown to co-ordinate one zinc atom each (denoted Zn4, Zn5, Zn6, respectively), as indicated (63).

where a gene for the expression of ZCCHC4-GFP was inserted, by site-specific recombination, into the genome of an engineered HEK-293-derived human cell line (Flp-In T-REx HEK-293), with the expression governed by a Dox inducible promoter. Reassuringly, the incubation of the cells with Dox induced the expression of the ZCCHC4-GFP fusion protein (Supplementary Figure S1). Fluorescence microscopy revealed that ZCCHC4-GFP was localized to large structures in the nucleus, resembling nucleoli (Figure 2A). The nucleolar localisation was further confirmed by demonstrating that the ZCCHC4-GFP fusion protein co-localized with the ribosomal protein RPL3, which has been reported to accumulate in the nucleolus (66).

ZCCHC4 interacts with proteins involved in RNA metabolism

To further explore the function of ZCCHC4, we performed a quantitative mass spectrometry (MS) based screen to uncover its interactome (Figure 2B). To this end, ZCCHC4-GFP was purified from the previously described ZCCHC4-GFP-expressing HEK-293-derived cell line and the associated proteins were quantified by protein mass spectrometry. To discriminate between proteins enriched by the bait

and the beads, or affinity tag, we used a corresponding cell line overexpressing GFP alone as control (Figure 2B). Proteins that were specifically enriched by ZCCHC4-GFP relative to the GFP control are in the following referred to as ZCCHC4 interactants, although it should be noted that this experimental setup not only allows for identification of direct protein-protein interactions but also detects indirect interactions mediated by proteins or nucleic acids. For the ZCCHC4 interactants, gene ontology terms related to the nucleolus, the ribosome and RNA metabolism were most strongly enriched (Figure 2C). Notably, the enrichment of nucleolar proteins is in good agreement with the observed nucleolar localization of the protein. Particularly interesting enriched proteins include the components of the so-called ASC-1 complex (ASCC1,2,3, and TRIP4), as well as the m^6A-reader YTHDC2. Interestingly, the two highly similar proteins AHCYL1 and AHCYL2 (*S*-adenosylhomocysteine hydrolase-like proteins 1 and 2) were also identified as ZCCHC4 interactants. These proteins show sequence similarity to *S*-adenosylhomocysteine hydrolase (AHCY), which plays an important role in removing *S*-adenosylhomocysteine, the inhibitory byproduct in AdoMet dependent MTase reactions. In summary, the interaction network suggests that ZCCHC4 is involved in
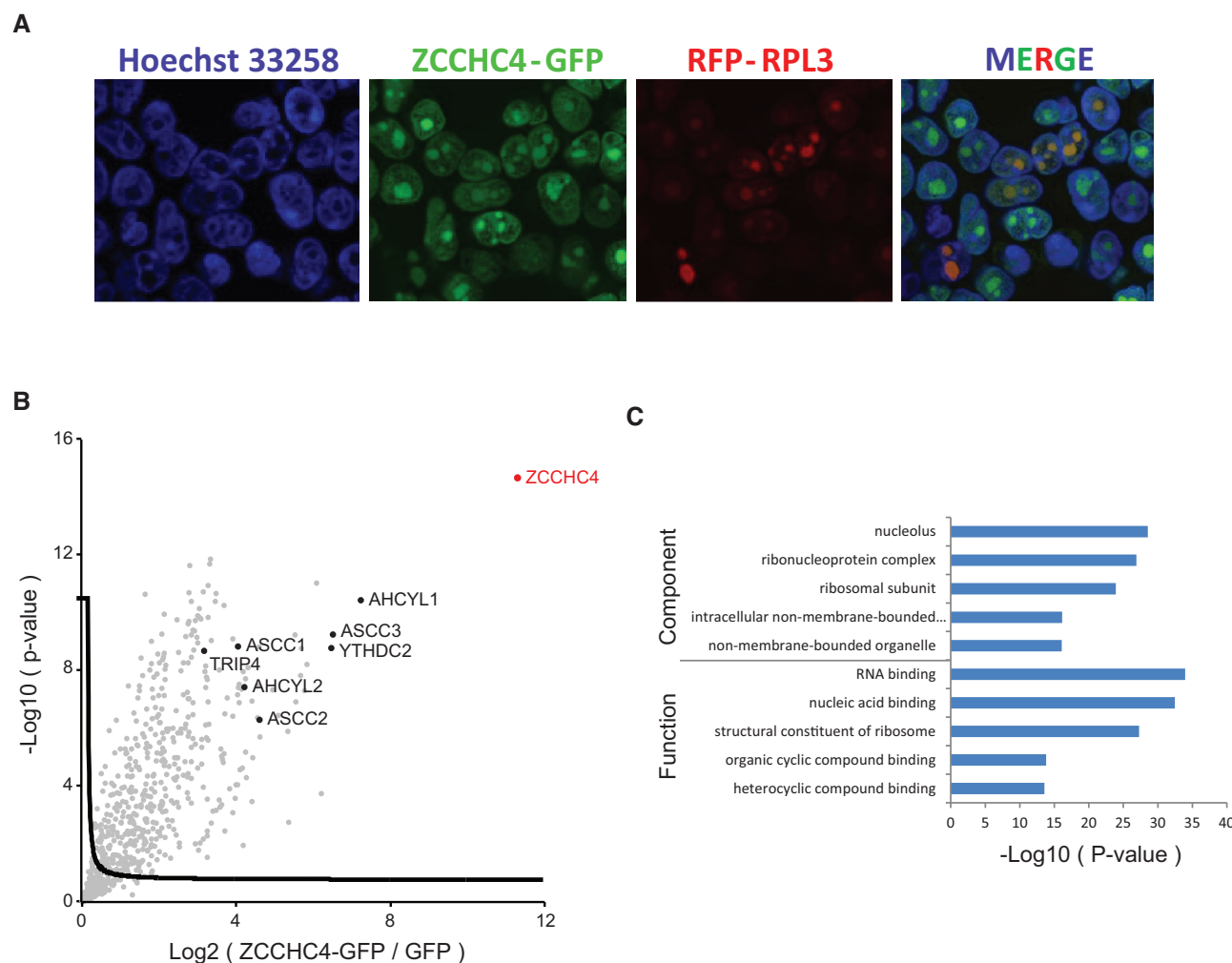
Figure 2. Subcellular localisation and interactome of ZCCHC4. (**A**) ZCCHC4 localises to nucleoli. HEK-293-derived cells stably expressing a ZCCHC4-GFP fusion protein were subjected to confocal fluorescence microscopy. ZCCHC4-GFP is shown in green, and Hoechst 33258 staining (blue) was used to visualize nuclei. RFP-RPL3 (red), expressed from a transiently transfected plasmid, was used as a marker for nucleoli. A merged image (right) shows co-localisation of ZCCHC4-GFP and RFP-RPL3 in the nucleus. (**B**) ZCCHC4 interactome. Volcano plot representation of proteins enriched by ZCCHC4-GFP versus GFP alone is shown. The curved line represents the significance cut-off (FDR = 0.01 and $s_0 = 0.1$). (**C**) Gene ontology analysis of ZCCHC4 interactants. Cellular functions and components (gene ontology terms) over-represented among the ZCCHC4 interactants are shown. The analysis was performed using GOrilla (59).

RNA metabolism and possibly in ribosome biogenesis in the nucleolus.

ZCCHC4 is required for the formation of m⁶A in 28S rRNA

The presence of a DPPF motif in ZCCHC4 indicated nucleic acid methylation as its most likely function (see above and Figure 1). Furthermore, the abundance of RNA-binding proteins in the ZCCHC4 interactome (Figure 2), suggested a role in RNA metabolism. Based on this, we assessed the levels of various methyl modifications in RNA from *ZCCHC4* KO HAP-1 cells through analyzing the RNA nucleoside composition by MS. Strikingly, we saw a substantial reduction (30–40%) in the overall levels of m⁶A in total RNA from the KO cells, relative to the corresponding 'wild-type' (WT) cells, whereas the levels of a number of other methylated nucleosides, including the adenoside derivatives 1-methyladenosine (m¹A) and N^6,N^6-dimethyladenosine (m⁶₂A) were unchanged (Figure 3A and data not shown). This indicated that ZCCHC4 is responsible for a substantial fraction of m⁶A in human RNA. To further identify the targeted RNA species, we assessed the m⁶A levels in large (>∼200 nt), small (<∼200 nt) and polyA-containing mRNAs. Clearly, the m⁶A levels in large RNAs were substantially reduced by *ZCCHC4* KO, whereas m⁶A in small RNAs and polyA-RNA was not significantly altered (Figure 3B).

Ribosome assembly and maturation occurs mainly in the nucleolus, and rRNAs account for the vast majority of large RNA within a eukaryotic cell. Thus, the substantial reduction in m⁶A in large *ZCCHC4* KO RNAs, taken together with ZCCHC4's nucleolar localisation and interactome, suggested its involvement in rRNA methylation. Hence, we next applied preparative size-exclusion chromatography to separate 18S rRNA and 28S rRNA, and measured the m⁶A levels in these rRNA species. Whereas m⁶A in 18S rRNA
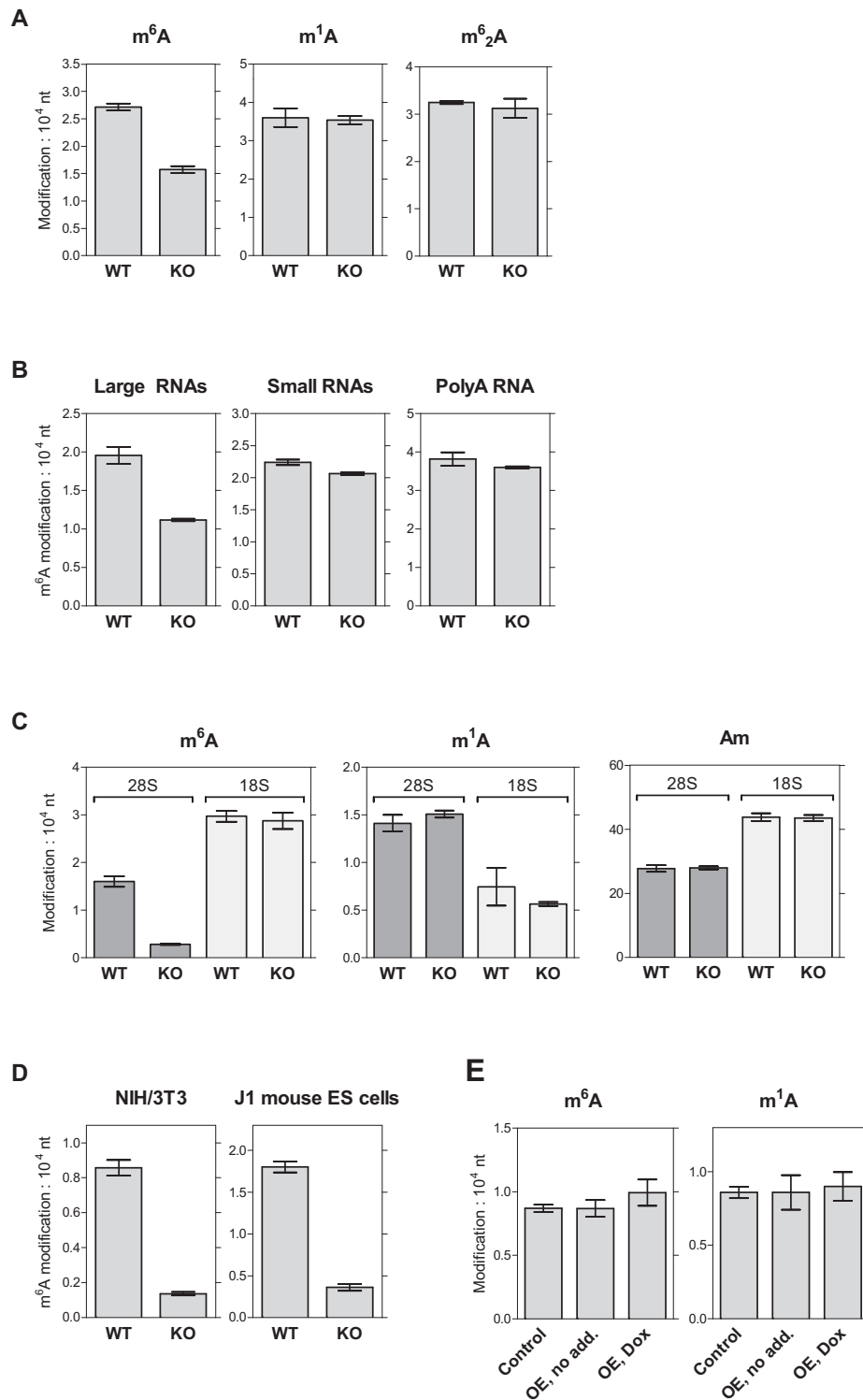
Figure 3. ZCCHC4 is required for formation of m^{6}A in mammalian 28S rRNA. The indicated RNA species were enzymatically digested to nucleosides, and various methylated nucleosides were quantified by LC–MS/MS. (**A**) Ablation of human ZCCHC4 in HAP-1 cells reduces m^{6}A levels in total RNA. Shown are results of the analysis of the methylated adenosine derivatives m^{6}A, m^{1}A and m$^6_2$A. (**B**) ZCCHC4 ablation specifically diminishes m^{6}A levels in large RNAs. Small RNAs, large RNAs and polyA-containing mRNAs were isolated as described in Materials and Methods. (**C**) Ablation of ZCCHC4 strongly diminishes m^{6}A in 28S rRNA. 18S and 28S rRNA were separated by size-exclusion chromatography as shown in Supplementary Figure S2, and the relevant fractions subjected to nucleoside analysis. (**D**) Ablation of mouse Zcchc4 in K:Molv NIH/3T3 and J1 mouse ES cells strongly diminishes m^{6}A in 28S rRNA. 28S rRNA containing fractions were isolated and analysed as in (C). (**E**) Overexpression of ZCCHC4-GFP in human HEK-293-derived cells has no appreciable effect on m^{6}A levels in 28S rRNA. OE indicates that HEK-293-derived cells engineered to over-express ZCCHC4 under a Dox-inducible promoter were used (see also Supplementary Figure S1). 'Dox' indicates that doxycyclin was added to induce transgene expression, whereas 'no add.' indicates that no doxycycline was added. 'Control' represents parental HEK-293 cells without the *ZCCHC4-GFP* transgene.

showed similar levels between the WT and KO cells, m⁶A in 28S rRNA was almost completely abolished in the KO (i.e. reduced to ~15% of WT levels) (Figure 3C). As our separation scheme does not completely separate 18S rRNA and 28S rRNA (Supplementary Figure S2), the remaining m⁶A observed in the 28S rRNA likely represents contamination by 18S rRNA, and the data suggest that ZCCHC4 is required for all m⁶A formation in 28S rRNA.

Conceivably, the observed effect of *ZCCHC4* KO on m⁶A levels in rRNA may be unrelated to ZCCHC4, and caused by an off-target inactivation of a different gene. To exclude this possibility, we investigated m⁶A levels in 28S rRNA from two additional, independently generated *Zcchc4* KO mouse cell lines, K:Molv NIH/3T3 fibroblasts and J1 ES cells. Reassuringly, a strong reduction in m⁶A in 28S rRNA was observed also in these KO cells (Figure 3D). We also considered the possibility that ZCCHC4-mediated methylation of 28S rRNA is sub-stoichiometric and limited by ZCCHC4 levels. If so, increasing ZCCHC4 expression would lead to increased m⁶A in 28S rRNA, and we thus investigated the effects of inducible overexpression of ZCCHC4-GFP on m⁶A in rRNA, using the HEK-293-derived cells described above (Figure 2A; Supplementary Figure S1). However, ZCCHC4-GFP over-expression did not significantly alter the level of m⁶A in 28S rRNA in these cells (Figure 3E), suggesting that the corresponding site is already fully modified in the non-overexpressing (non-induced) cells. Taken together, the above results demonstrate that ZCCHC4 is required for the formation of m⁶A in mammalian 28S rRNA.

ZCCHC4 mediates methylation at A4220 in 28S rRNA in cells

Several studies have shown that 28S rRNA from vertebrates contains a single m⁶A residue. This modification site is localized at the position originally referred to as A4190 (67–69), but as A4220 in a recently introduced alternative numbering system (32,70). We have here chosen to use the latter nomenclature, since this was used by two very recent studies that, similarly to us, investigated the role of ZCCHC4 in 28S rRNA methylation (see Discussion) (71,72). Similar to the residues targeted by other snoRNA-independent MTases, A4220 is localized to a central part of the 28S rRNA, close to the active centre of the ribosome (Figure 4A) (32). A4220 is localized within the loop region of a predicted stem–loop structure, and interacts, in the context of the intact ribosome, with C4211, found at the opposite side of the loop (Figure 4B) (32). Interestingly, the equivalent base pair in the yeast ribosome also contains a methyl-modified base, but here the methylation is found on the opposite base, an example of so-called reciprocally methylated base pairs from different taxonomic groups (32).

To directly establish that ZCCHC4 is required for the methylation of A4220, we isolated an ~50 nucleotide 28S rRNA sub-fragment harbouring A4220 from WT or *ZCCHC4* KO HAP-1 cells, followed by digestion with RNase T1. The resulting products were then analysed by MALDI-MS. Indeed, the A4220 encompassing RNase T1 product from WT cells showed a molecular mass corresponding to the expected m⁶A modification, whereas the mass

of the corresponding *ZCCHC4* KO fragment was 14.0 Da lower, i.e. corresponding to the unmethylated form (Figure 4C). MS/MS fragmentation patterns further confirmed the identity of the fragments, and that A4220 is the site of ZCCHC4-dependent methylation (Supplementary Figure S3). Notably, we did not observe a signal corresponding to unmethylated A4220 in the WT cells, suggesting that this site is fully m⁶A-modified. Together with the nucleoside analyses, these results firmly establish that ZCCHC4 is required for the methylation of 28S rRNA at A4220 in cells.

Recombinant ZCCHC4 mediates methylation of the A4220-containing stem–loop *in vitro*

The above results demonstrated that ZCCHC4 is required for the formation of m⁶A4220, and we next investigated whether recombinant ZCCHC4 is capable of catalysing the corresponding reaction *in vitro*. To this end, a 5′-biotinylated RNA oligonucleotide corresponding to the A4220-encompassing stem–loop was incubated with recombinant ZCCHC4 in the presence of [³H]AdoMet, and the incorporation of radioactivity into RNA was measured after streptavidin-mediated pulldown of the RNA substrate. Clearly, ZCCHC4 mediated robust RNA methylation of the unmethylated A4220 oligonucleotide (100× above background levels) (Figure 5). In contrast, no enzymatic activity was observed when a putatively inactive mutant enzyme, mutated within the conserved DPPF motif (D276A; Figure 1A,B), was used (Figure 5). Importantly, when a corresponding m⁶A4220-modified oligonucleotide was used, methylation was abolished, indicating that the observed activity represents methylation at A4220. These results show that ZCCHC4 directly catalyses AdoMet-dependent formation of m⁶A4220 in 28S rRNA, and indicate that ZCCHC4 is a stand-alone enzyme not requiring additional partners or cofactors.

Identification of proteins that show methylation-status-sensitive binding to the A4220-encompassing stem–loop

We reasoned that the m⁶A-modification in 28S rRNA may mediate or prevent specific rRNA-protein interactions. To explore this, we performed a quantitative proteomics experiment where proteins were pulled-down from a HeLa extract using as bait the RNA oligonucleotide encompassing the m⁶A4220-containing stem–loop, or a corresponding unmodified RNA. To quantitatively compare the interactants pulled down with the two probes, proteins were digested to peptides that were labelled with isotopically labelled dimethyl moieties [heavy (H) or light (L)], followed by MS-based quantitation. Both a 'forward' and a 'reverse' (label-swap) pulldown were performed, and in a logarithmic plot of reverse versus forward H/L ratios, proteins that are enriched or depleted by the presence of m⁶A in the RNA bait are found in the upper right or lower left quadrants, respectively (Supplementary Figure S4). The shape of the plot was somewhat asymmetric, with eight proteins being depleted by the presence of m⁶A (within the applied threshold, see Supplementary Figure S4), but with no proteins identified as significantly enriched by the m⁶A-containing bait. Interestingly, the eight depleted proteins encompassed proteins
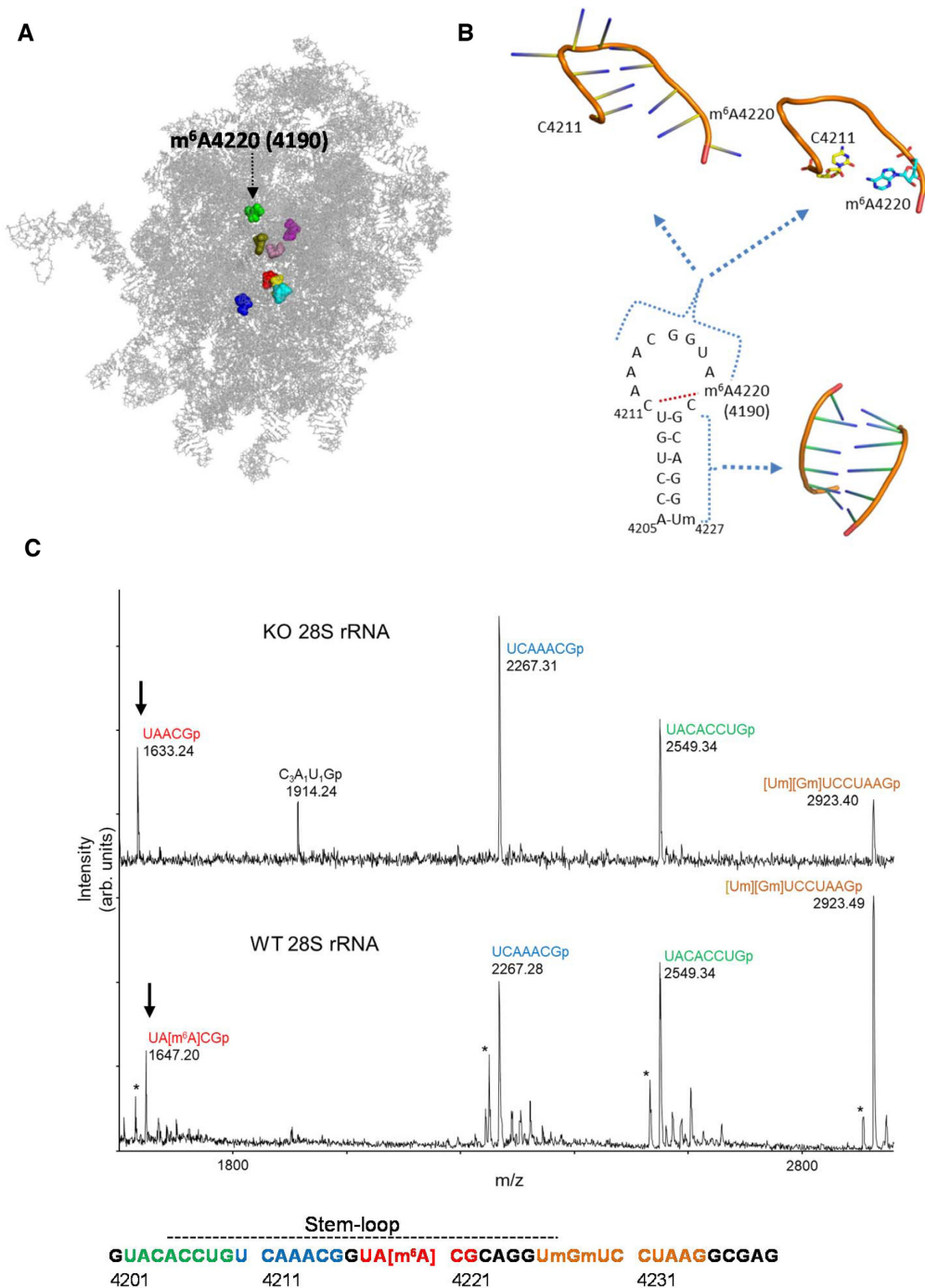
Figure 4. ZCCHC4-dependent methylation of A4220 in 28S rRNA in cells. (**A**) Localization of m^{6}A4220 in the 28S RNA structure. m^{6}A4220 (green) is shown on the 28S rRNA structure, together with other known, snoRNA-independent methyl modifications (m^{1}A1322, purple; m^{3}C3782, blue; Gm4196, olive; m^{5}C4447, pink; Um4498, cyan; Gm4499, yellow; m^{3}U4530, red). The figure was adapted from Sergiev *et al.* (32), and made based on the corresponding published structure (32) (PDB ID: 4UG0). Note that m^{6}A4220, by an alternative numbering system, previously has been referred to as m^{6}A4190. (**B**) Structure of the A4220-containing stem–loop. Shown is a schematic representation of the stem–loop, based on secondary structure prediction, as well as the structure of the corresponding segments in the context of the intact ribosome (generated from PDB ID: 4UG0; shown with orange backbone). Also indicated are the previously reported proximity and interaction between A4220 and C4211 (shown as stick representation in upper right panel, and indicated by a red, dotted line on the cartoon representation of the sequence) (32). (**C**) ZCCHC4 is required for methylation of A4220. 28S rRNA sub-fragment isolated from *ZCCHC4* KO HAP-1 cells or corresponding WT cells was digested with RNase T1, and the resulting products analysed by MALDI mass spectrometry. Peaks corresponding to products derived from the A4220-containing stem–loop are indicated. Arrows indicate the A4220-encompassing product. Asterisks indicate 2′-3′ cyclic phosphate intermediates from the RNase T1 digestion. The *m/z* 1914.2 fragment was occasionally observed in both WT and KO rRNA preparations (but was detected only in the KO preparation in the shown experiment). Sequence information was not obtained, but the calculated stoichiometry (C$_3$A$_1$U$_1$Gp) suggests that this fragment represents a truncated version, CACCUGp, of the *m/z* 2549.34 RNase T1 digestion product (shown in green); heterogeneity at the termini is commonly observed with this approach to purify rRNA sub-fragments. Um and Gm are 2′-*O*-ribose methylated versions of U and G, respectively.
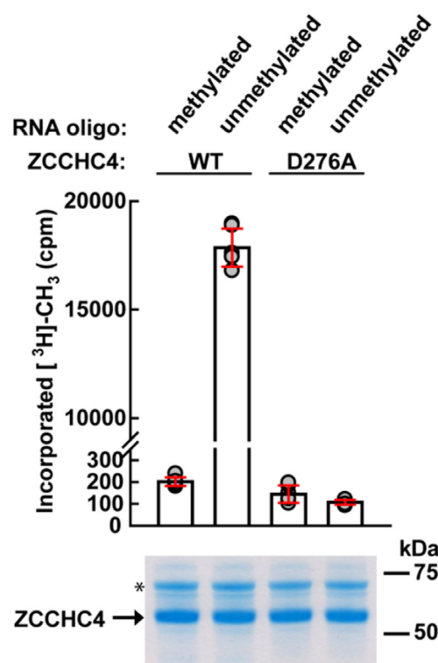
Figure 5. ZCCHC4-mediated methylation of the A4220-encompassing stem–loop *in vitro*. Wild-type recombinant ZCCHC4, or a putatively enzymatically inactive mutant (D276A) was incubated with a 5′-biotinylated, non-methylated RNA-oligonucleotide encompassing the A4220-containing stem–loop (representing nucleotides 4204 – 4228 in 28S rRNA) in the presence of [^{3}H]AdoMet. The corresponding oligonucleotide containing an m^{6}A modification at position A4220 represented a negative control. The oligonucleotide was subsequently pulled down from the reaction mixture using streptavidin-coated beads, and incorporated radioactivity measured by scintillation counting. Red whiskers indicate S.D., n=6. Purity and integrity of recombinant enzymes was assessed by Coomassie-stained SDS-PAGE of an aliquot of the reaction mixture (lower panel). The asterisk indicates a co-purifying *E. coli* protein that by mass spectrometry was identified as ArnA (bifunctional polymyxin resistance protein), which was reported as a common contaminant in His-tag affinity purifications (83).

involved in ribosome biogenesis and assembly (Supplementary Figure S4). This included DKC1 (dyskerin), which is the catalytic component of the H/ACA ribonucleoprotein (RNP) complex responsible for introducing pseudouridine into rRNA (73). A second identified protein, NAF1, is required for assembly of this complex, but the significance of this finding remains uncertain as NAF1 is excluded from nucleoli (74). Moreover, HNRNP-U, which is a well-studied RNA-binding protein mainly implicated in gene regulation and chromatin organisation, but which has also been observed in nucleoli (75), was found to be repelled by the m^{6}A modification. Albeit below the applied threshold level, 6–7 proteins stood out as being attracted by the m^{6}A modification. Interestingly, these included all the three canonical m^{6}A readers of the YTHDF subgroup, i.e. YTHDF1, YTHDF2 and YTHDF3, but otherwise no proteins with obvious links to the ribosome or to RNA metabolism. The functional significance of the above data is unclear, but they may suggest that A4220 methylation status influences interactions between proteins and the A4220-encompassing stem–loop during ribosome maturation.

The absence of m^{6}A4220 perturbs ribosomal translation dynamics

To investigate the functional role of ZCCHC4-mediated methylation of 28S rRNA in translation, we performed ribosome profiling experiments in HAP-1 cells, comparing the *ZCCHC4* KO and WT cells. Ribosome profiling is a method to quantitatively analyse translation dynamics *in vivo* at codon resolution (76). One feature of global translation dynamics is the time ribosomes spend for translating specific codons. The duration of a decoding cycle depends, e.g. on tRNA modifications and the modification of elongation factors, such as eEF1A, and affects protein homeostasis and mRNA turnover (37,41,57,77,78). This is estimated by analyzing codon-specific ribosomal A-site occupancy of individual codons. By normalizing for codon usage in the transcripts that are expressed, the frequency of a codon in the A-site can be used as a proxy for the time ribosomes spend at translating this codon. Interestingly, when comparing codon occupancy in the *ZCCHC4* KO cells relative to the WT, we observed a striking difference of ribosomal occupancy for some codons (Figure 6A). For example, GAA, TAC, TGG and TTG were enriched in the KO A-site, while ATT, CCC, CCT, GGA and GTA are found less frequently (Figure 6A). No such effect was observed for the +1-codon, which has not been translated by the ribosome at the moment of cell lysis, and thus represents a control.

Recently, Grosjean and Westhof proposed a new circular representation of the genetic code, based on the energies of the corresponding codon-anticodon interactions, thereby integrating the current knowledge on the decoding process (79). Interactions involving only G or C in the first two nucleotides of the codon are considered 'STRONG', those involving only A or T are considered 'WEAK', whereas the remaining ones are classified as 'INTERMEDIATE' (Figure 6B). We used this codon wheel representation to visualize the codons that where most strongly affected by *ZCCHC4* KO in the RP experiments, i.e. those that showed the largest difference between their relative A-site and +1-site occupancies. Thus, we selected the 10 codons that showed the largest increase in occupancy as well as the 10 codons that showed the largest decrease (Figure 6B). Strikingly, all the five codons that fell into the STRONG category showed decreased codon occupancy, whereas the six out of the seven codons in the WEAK category showed increased occupancy. This suggests that the strength of the codon-anticodon interaction influences how ZCCHC4-mediated rRNA modification affects mRNA translation (see also Discussion).

Codon usage is not random but differs between organisms, tissues, and functional categories of genes/proteins (80). Consequently, we reasoned that the observed codon-specific effects of *ZCCHC4* KO will likely also be manifested at the gene level. Thus, we also calculated differential mRNA translation between the *ZCCHC4* KO and WT using our ribosomal profiling data. We observed an upregulation of genes representing processes related to RNA metabolism and the nucleosome, whereas genes related to signal transduction and neural development were amongst the downregulated ones (Figure 6C, D). Taken together, our results indicate that ribosomes lacking the m^{6}A
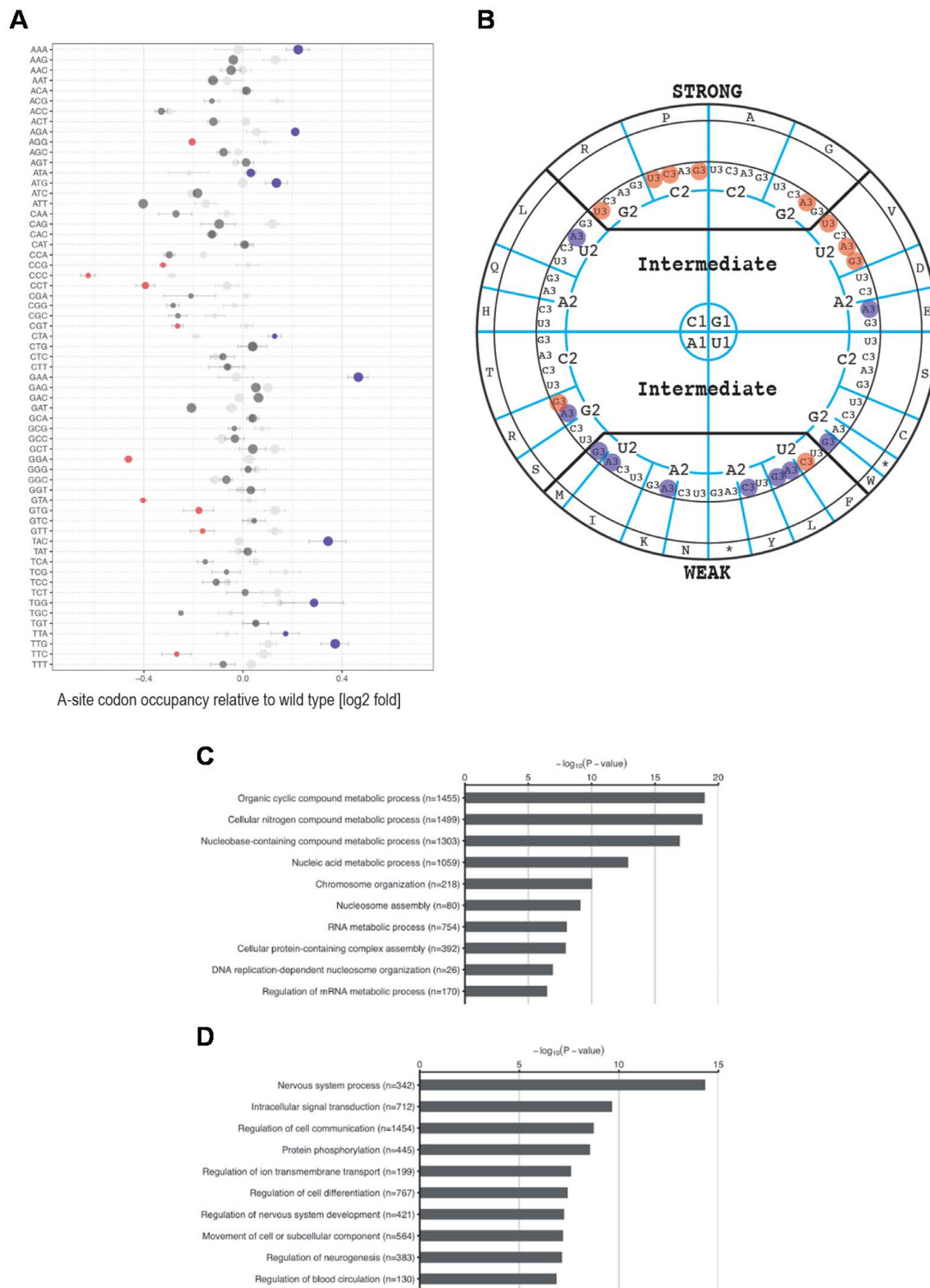
Figure 6. Ribosomes in ZCCHC4-deficient cells exhibit altered translation. (**A**) Relative ribosome occupancy of each codon in WT cells relative to *ZCCHC4* KO cells. A-site occupancy (blue, red and dark grey circles) and +1-site occupancy (light grey circles) were normalized to (not yet translated) downstream codons (mean ± S.D., n = 3). The A-site occupancy of the 10 codons that showed the largest increase (calculated as the difference between the relative A-site and +1-site occupancies) is indicated by blue circles; the 10 codons that showed the largest decrease are shown as red circles, and remaining codons as dark grey circles. Circle size indicates the relative frequency of codons in quartiles (larger is more frequent). (**B**) Codon wheel representation of strongly affected codons. The 20 codons most affected by *ZCCHC4* KO in (A) have been indicated (using the same color code) on a codon wheel representation of the genetic code, based on anticodon-codon interaction strengths (STRONG, WEAK or INTERMEDIATE), as proposed by Grosjean and Westhof (79). The figure was adapted from (79). (**C**) Gene ontology (GO) term analysis (Cellular Process) of genes significantly upregulated in *ZCCHC4* deficient cells on the footprint level. Numbers in brackets indicate the genes matching the respective GO term category. (**D**) As in (C), but for significantly downregulated genes.

modification of 28S rRNA exhibit deviating translation activity.

The observed effects of *ZCCHC4* KO on mRNA translation may be directly caused by the absence of methylation at A4220. However, lack of methylation may also affect the assembly and maturation of the ribosome, so that the observed translation effect may be due to an aberrant ribosome, rather than the specific lack of m⁶A4220. To explore the possible role of ZCCHC4 in ribosome maturation, we investigated by northern blotting the kinetics of rRNA processing in HAP-1 cells but did not observe any differences between *ZCCHC4* KO and WT cells (Supplementary Figure S5). We also investigated by sucrose gradient density centrifugation, the relative distribution of polysomes versus monosomes in WT and *ZCCHC4* KO HAP-1 cells, but did not detect any differences (Supplementary Figure S5F). Furthermore, to investigate possible effects of *ZCCHC4* KO on ribosome assembly, we performed a quantitative proteomics analysis of translating ribosomes from these cells, but again without observing any significant differences between the KO and WT cells (Supplementary Figure S6). Taken together, these results indicates that *ZCCHC4* KO does not substantially affect ribosome maturation and assembly, and may suggest that the deviating translation in the *ZCCHC4* KO cells may reflect a direct effect on mRNA translation of the lack of methylation of 28S rRNA at A4220.

DISCUSSION

We have here investigated the function of the human MTase ZCCHC4. We found that *ZCCHC4* KO in HAP-1 cells abrogated m⁶A modification of A4220 (alternatively referred to as A4190) in 28S rRNA, and that recombinant ZCCHC4 showed robust methylation activity on an RNA oligonucleotide encompassing the methylation site. Taken together, this firmly established ZCCHC4 as the enzyme responsible for introducing the single m⁶A modification present in 28S rRNA. Moreover, we observed that ZCCHC4 is localized to the nucleolus, the primary location of ribosome synthesis, assembly and maturation, and ZCCHC4 was found to interact with a number of RNA-binding proteins. Finally, *ZCCHC4* KO cells displayed altered translation dynamics, demonstrating a functional significance of ZCCHC4-mediated methylation of rRNA.

Codon-specific effects of *ZCCHC4* KO on mRNA translation

In ribosomal profiling experiments, we observed that *ZCCHC4* KO affected the occupancy at several different codons during translation (Figure 6A). Moreover, many of the codons that showed the strongest increase in occupancy (i.e. reduction of translation speed) in the *ZCCHC4* KO cells have a weak codon-anticodon interaction, whereas several of those that showed the largest decrease in occupancy (i.e. increase of translation speed) have a strong interaction (Figure 6B). Only a subset of the codons in the STRONG and WEAK groups (Figure 6B) showed this effect, and the underlying mechanism remains elusive, but we still find it important to share this observation. Moreover,

the interactions occurring between the ribosomal A-site and the helix formed by the anticodon/codon, referred to as the 'ribosomal grip', can vary between different codons (79). Thus, one may speculate that effects of m⁶A4220 methylation on the ribosomal grip may underlie the observed codon-specific effects of *ZCCHC4* KO on mRNA translation. It may be interesting to study translation dynamics of m⁶A4420-deficient ribosomes *in vitro* to determine the exact step in the elongation cycle that is affected by the lack of this modification.

Comparison with other studies on ZCCHC4-mediated rRNA methylation

While this manuscript was in preparation, Ma *et al.* reported results similar to those obtained herein, i.e. they showed, using somewhat different experimental approaches, that ZCCHC4 is responsible for installing m⁶A at A4220 (72). Moreover, another relevant study appeared during the revision of our manuscript; van Tran *et al.*, established METTL5 as the MTase responsible for m⁶A modification of 18S rRNA, but also showed that *ZCCHC4* KO abolished m⁶A modification of 28S rRNA (71). Interestingly, all three studies (Ma *et al.*, van Tran *et al.*, and our study) have investigated various functional effects of *ZCCHC4* KO, particularly related to the ribosome and mRNA translation. We observed gene- and codon-specific effects of *ZCCHC4* KO on mRNA translation in ribosomal profiling experiments (Figure 6), whereas Ma *et al.* performed sequencing of polysome-associated mRNAs, and observed a broader mRNA(polysome)/mRNA(input) profile in the *ZCCHC4* KO cells, indicating a reduction of translational control (72). Furthermore, Ma *et al.* compared WT and *ZCCHC4* KO cells in polysome profiling experiments, and found that the polysome/monosome ratio was reduced in the *ZCCHC4* KO cells (72), whereas we, as well as van Tran *et al.*, did not observe any such difference (Supplementary Figure S5F) (71). Both van Tran *et al.* and we compared the kinetics of rRNA processing in WT and *ZCCHC4* KO cells but neither study demonstrated any difference (Supplementary Figure S5) (71). Moreover, we investigated by proteomics the protein composition of translating ribosomes, and found no significant differences between WT and KO cells (Supplementary Figure S6). Although there are some differences between the results from the three studies, possibly reflecting that different cell lines were used, the conclusion may be drawn that ZCCHC4-mediated methylation appears to play an important role in the process of mRNA translation, but is less important for ribosome assembly and maturation.

Role of ZCCHC4 in cell growth and cancer

Interestingly, the study by Ma *et al.* implicated ZCCHC4 in cancer cell growth and tumour progression. They found that *ZCCHC4* KO diminished the growth of the liver cancer cell line HepG2 both in tissue culture and as tumour xenografts in mice (72). Furthermore, higher levels of ZCCHC4 protein and m⁶A in 28S rRNA were observed in liver cancer tissue compared to surrounding, healthy tissue (72). In contrast, van Tran *et al.* did not see any effect of *ZCCHC4* KO on the growth of HCT116 cells (71). However,

there are indications that the level of m^{6}A in 28S rRNA may vary between different cell lines. Our data suggested near-complete methylation of A4220 in HEK-293 cells and HAP-1 cells (Figure 3E and Figure 4C, respectively), and Taoka *et al.* also observed complete methylation in human TK6 and HeLa cells (30). In contrast, Ma *et al.* found only ∼55% methylation in HepG2 cells. Possibly, such variations underlie the observed variations in the phenotypic effects of *ZCCHC4* KO between different cell lines.

Additional evidence for a role of ZCCHC4 in cancer comes from two studies that implicated mouse Zcchc4 in K-Ras mediated epigenetic gene silencing of the FAS gene (81,82). FAS is an important mediator of apoptosis, and knock-down of Zcchc4 in mouse cells caused reactivation of FAS expression, as well as loss of DNA methylation at its promoter (81,82). However, a role for ZCCHC4 in epigenetics and gene regulation is not readily linked to its observed rRNA MTase activity. The recent study by van Tran *et al.* investigated m^{6}A modification transcriptome-wide in KO and WT HCT-116 cells, and A4220 in 28S rRNA was found to be the only differentially modified site (71). Thus, there are no indications that ZCCHC4 has substrates other than 28S rRNA, and its potential role in epigenetic gene silencing remains elusive.

DATA AVAILABILITY

Proteome data for the ZCCHC4-pulldown (Figure 2), m^{6}A-RNA-pulldown (Supplementary Figure S4), and polysome proteomics (Supplementary Figure S6) experiments are available at ProteomeExchange (http://www.proteomexchange.org/) with accession numbers PXD012346, PXD013354 and PXD015084 respectively. The ribosome profiling experiments (Figure 6) are available at the Gene Expression Omnibus with accession number GSE128994.

SUPPLEMENTARY DATA

Supplementary Data are available at NAR Online.

REFERENCES

1. Helm,M. and Alfonzo,J.D. (2014) Posttranscriptional RNA modifications: playing metabolic games in a cell's chemical Legoland. *Chem. Biol.*, **21**, 174–185.
2. Agris,P.F. (2004) Decoding the genome: a modified view. *Nucleic Acids Res.*, **32**, 223–238.
3. Motorin,Y. and Helm,M. (2011) RNA nucleotide methylation. *Wiley. Interdiscip. Rev. RNA.*, **2**, 611–631.
4. Desrosiers,R., Friderici,K. and Rottman,F. (1974) Identification of methylated nucleosides in messenger RNA from Novikoff hepatoma cells. *Proc. Natl. Acad. Sci. U.S.A.*, **71**, 3971–3975.
5. Perry,R.P., Kelley,D.E., Friderici,K. and Rottman,F. (1975) The methylated constituents of L cell messenger RNA: evidence for an unusual cluster at the 5′ terminus. *Cell*, **4**, 387–394.
6. Bokar,J.A., Shambaugh,M.E., Polayes,D., Matera,A.G. and Rottman,F.M. (1997) Purification and cDNA cloning of the AdoMet-binding subunit of the human mRNA (N6-adenosine)-methyltransferase. *RNA*, **3**, 1233–1247.
7. Clancy,M.J., Shambaugh,M.E., Timpte,C.S. and Bokar,J.A. (2002) Induction of sporulation in Saccharomyces cerevisiae leads to the formation of N6-methyladenosine in mRNA: a potential mechanism for the activity of the IME4 gene. *Nucleic Acids Res.*, **30**, 4509–4518.
8. Dominissini,D., Moshitch-Moshkovitz,S., Schwartz,S., Salmon-Divon,M., Ungar,L., Osenberg,S., Cesarkas,K., Jacob-Hirsch,J., Amariglio,N., Kupiec,M. *et al.* (2012) Topology of the human and mouse m6A RNA methylomes revealed by m6A-seq. *Nature*, **485**, 201–206.
9. Meyer,K.D., Saletore,Y., Zumbo,P., Elemento,O., Mason,C.E. and Jaffrey,S.R. (2012) Comprehensive analysis of mRNA methylation reveals enrichment in 3′ UTRs and near stop codons. *Cell*, **149**, 1635–1646.
10. Zaccara,S., Ries,R.J. and Jaffrey,S.R. (2019) Reading, writing and erasing mRNA methylation. *Nat. Rev. Mol. Cell Biol.*, **20**, 608–624.
11. Roundtree,I.A., Luo,G.Z., Zhang,Z., Wang,X., Zhou,T., Cui,Y., Sha,J., Huang,X., Guerrero,L., Xie,P. *et al.* (2017) YTHDC1 mediates nuclear export of N(6)-methyladenosine methylated mRNAs. *Elife*, **6**, e31311.
12. Wang,X., Lu,Z., Gomez,A., Hon,G.C., Yue,Y., Han,D., Fu,Y., Parisien,M., Dai,Q., Jia,G. *et al.* (2014) N6-methyladenosine-dependent regulation of messenger RNA stability. *Nature*, **505**, 117–120.
13. Wang,X., Zhao,B.S., Roundtree,I.A., Lu,Z., Han,D., Ma,H., Weng,X., Chen,K., Shi,H. and He,C. (2015) N(6)-methyladenosine modulates messenger RNA translation efficiency. *Cell*, **161**, 1388–1399.
14. Xiao,W., Adhikari,S., Dahal,U., Chen,Y.S., Hao,Y.J., Sun,B.F., Sun,H.Y., Li,A., Ping,X.L., Lai,W.Y. *et al.* (2016) Nuclear m(6)A Reader YTHDC1 regulates mRNA splicing. *Mol. Cell*, **61**, 507–519.
15. Liu,J., Yue,Y., Han,D., Wang,X., Fu,Y., Zhang,L., Jia,G., Yu,M., Lu,Z., Deng,X. *et al.* (2014) A METTL3-METTL14 complex mediates mammalian nuclear RNA N6-adenosine methylation. *Nat. Chem. Biol.*, **10**, 93–95.
16. Ping,X.L., Sun,B.F., Wang,L., Xiao,W., Yang,X., Wang,W.J., Adhikari,S., Shi,Y., Lv,Y., Chen,Y.S. *et al.* (2014) Mammalian WTAP is a regulatory subunit of the RNA N6-methyladenosine methyltransferase. *Cell Res.*, **24**, 177–189.
17. Schwartz,S., Mumbach,M.R., Jovanovic,M., Wang,T., Maciag,K., Bushkin,G.G., Mertins,P., Ter-Ovanesyan,D., Habib,N., Cacchiarelli,D. *et al.* (2014) Perturbation of m6A writers reveals two distinct classes of mRNA methylation at internal and 5′ sites. *Cell Rep.*, **8**, 284–296.
18. Pendleton,K.E., Chen,B., Liu,K., Hunter,O.V., Xie,Y., Tu,B.P. and Conrad,N.K. (2017) The U6 snRNA m(6)A methyltransferase

METTL16 regulates SAM synthetase intron retention. *Cell*, **169**, 824–835.

19. Warda,A.S., Kretschmer,J., Hackert,P., Lenz,C., Urlaub,H., Hobartner,C., Sloan,K.E. and Bohnsack,M.T. (2017) Human METTL16 is a N(6)-methyladenosine (m(6)A) methyltransferase that targets pre-mRNAs and various non-coding RNAs. *EMBO Rep.*, **18**, 2004–2014.

20. Akichika,S., Hirano,S., Shichino,Y., Suzuki,T., Nishimasu,H., Ishitani,R., Sugita,A., Hirose,Y., Iwasaki,S., Nureki,O. *et al.* (2018) Cap-specific terminal N (6)-methylation of RNA by an RNA polymerase II-associated methyltransferase. *Science*, **363**, eaav0080.

21. Sun,H., Zhang,M., Li,K., Bai,D. and Yi,C. (2018) Cap-specific, terminal N(6)-methylation by a mammalian m(6)Am methyltransferase. *Cell Res.*, **29**, 80–82.

22. Li,A., Chen,Y.S., Ping,X.L., Yang,X., Xiao,W., Yang,Y., Sun,H.Y., Zhu,Q., Baidya,P., Wang,X. *et al.* (2017) Cytoplasmic m(6)A reader YTHDF3 promotes mRNA translation. *Cell Res.*, **27**, 444–447.

23. Shi,H., Wang,X., Lu,Z., Zhao,B.S., Ma,H., Hsu,P.J., Liu,C. and He,C. (2017) YTHDF3 facilitates translation and decay of N(6)-methyladenosine-modified RNA. *Cell Res.*, **27**, 315–328.

24. Kretschmer,J., Rao,H., Hackert,P., Sloan,K.E., Hobartner,C. and Bohnsack,M.T. (2018) The m(6)A reader protein YTHDC2 interacts with the small ribosomal subunit and the 5′-3′ exoribonuclease XRN1. *RNA*, **24**, 1339–1350.

25. Hsu,P.J., Zhu,Y., Ma,H., Guo,Y., Shi,X., Liu,Y., Qi,M., Lu,Z., Shi,H., Wang,J. *et al.* (2017) Ythdc2 is an N(6)-methyladenosine binding protein that regulates mammalian spermatogenesis. *Cell Res.*, **27**, 1115–1127.

26. Jia,G., Fu,Y., Zhao,X., Dai,Q., Zheng,G., Yang,Y., Yi,C., Lindahl,T., Pan,T., Yang,Y.G. *et al.* (2011) N6-methyladenosine in nuclear RNA is a major substrate of the obesity-associated FTO. *Nat. Chem. Biol.*, **7**, 885–887.

27. Zheng,G., Dahl,J.A., Niu,Y., Fedorcsak,P., Huang,C.M., Li,C.J., Vagbo,C.B., Shi,Y., Wang,W.L., Song,S.H. *et al.* (2013) ALKBH5 is a mammalian RNA demethylase that impacts RNA metabolism and mouse fertility. *Mol. Cell*, **49**, 18–29.

28. Pelletier,J., Thomas,G. and Volarevic,S. (2018) Ribosome biogenesis in cancer: new players and therapeutic avenues. *Nat. Rev. Cancer*, **18**, 51–63.

29. Piekna-Przybylska,D., Decatur,W.A. and Fournier,M.J. (2008) The 3D rRNA modification maps database: with interactive tools for ribosome analysis. *Nucleic Acids Res.*, **36**, D178–D183.

30. Taoka,M., Nobe,Y., Yamaki,Y., Sato,K., Ishikawa,H., Izumikawa,K., Yamauchi,Y., Hirota,K., Nakayama,H., Takahashi,N. *et al.* (2018) Landscape of the complete RNA chemical modifications in the human 80S ribosome. *Nucleic Acids Res.*, **46**, 9289–9298.

31. Watkins,N.J. and Bohnsack,M.T. (2012) The box C/D and H/ACA snoRNPs: key players in the modification, processing and the dynamic folding of ribosomal RNA. *Wiley. Interdiscip. Rev. RNA.*, **3**, 397–414.

32. Sergiev,P.V., Aleksashin,N.A., Chugunova,A.A., Polikanov,Y.S. and Dontsova,O.A. (2018) Structural and evolutionary insights into ribosomal RNA methylation. *Nat. Chem. Biol.*, **14**, 226–235.

33. Sharma,S. and Lafontaine,D.L.J. (2015) 'View From A Bridge': A New Perspective on Eukaryotic rRNA Base Modification. *Trends Biochem. Sci.*, **40**, 560–575.

34. Sloan,K.E., Warda,A.S., Sharma,S., Entian,K.D., Lafontaine,D.L.J. and Bohnsack,M.T. (2017) Tuning the ribosome: The influence of rRNA modification on eukaryotic ribosome biogenesis and function. *RNA. Biol.*, **14**, 1138–1152.

35. Petrossian,T.C. and Clarke,S.G. (2011) Uncovering the human methyltransferasome. *Mol. Cell Proteomics.*, **10**, M110.

36. Jakobsson,M.E., Moen,A., Bousset,L., Egge-Jacobsen,W., Kernstock,S., Melki,R. and Falnes,P.O. (2013) Identification and characterization of a novel human methyltransferase modulating Hsp70 function through lysine methylation. *J. Biol. Chem.*, **288**, 27752–27763.

37. Jakobsson,M.E., Malecki,J.M., Halabelian,L., Nilges,B.S., Pinto,R., Kudithipudi,S., Munk,S., Davydova,E., Zuhairi,F.R., Arrowsmith,C.H. *et al.* (2018) The dual methyltransferase METTL13 targets N terminus and Lys55 of eEF1A and modulates codon-specific translation rates. *Nat. Commun.*, **9**, 3411.

38. Kernstock,S., Davydova,E., Jakobsson,M., Moen,A., Pettersen,S., Maelandsmo,G.M., Egge-Jacobsen,W. and Falnes,P.O. (2012) Lysine methylation of VCP by a member of a novel human protein methyltransferase family. *Nat. Commun.*, **3**, 1038.

39. Leihne,V., Kirpekar,F., Vagbo,C.B., van den Born,E., Krokan,H.E., Grini,P.E., Meza,T.J. and Falnes,P.O. (2011) Roles of Trm9- and ALKBH8-like proteins in the formation of modified wobble uridines in Arabidopsis tRNA. *Nucleic Acids Res.*, **39**, 7688–7701.

40. Malecki,J., Ho,A.Y., Moen,A., Dahl,H.A. and Falnes,P.O. (2015) Human METTL20 is a mitochondrial lysine methyltransferase that targets the beta subunit of electron transfer flavoprotein (ETFbeta) and modulates its activity. *J. Biol. Chem.*, **290**, 423–434.

41. Malecki,J., Aileni,V.K., Ho,A.Y., Schwarz,J., Moen,A., Sorensen,V., Nilges,B.S., Jakobsson,M.E., Leidel,S.A. and Falnes,P.O. (2017) The novel lysine specific methyltransferase METTL21B affects mRNA translation through inducible and dynamic methylation of Lys-165 in human eukaryotic elongation factor 1 alpha (eEF1A). *Nucleic Acids Res.*, **45**, 4370–4389.

42. Songe-Moller,L., van den Born,E., Leihne,V., Vagbo,C.B., Kristoffersen,T., Krokan,H.E., Kirpekar,F., Falnes,P.O. and Klungland,A. (2010) Mammalian ALKBH8 possesses tRNA methyltransferase activity required for the biogenesis of multiple wobble uridine modifications implicated in translational decoding. *Mol. Cell Biol.*, **30**, 1814–1827.

43. Katoh,K., Misawa,K., Kuma,K. and Miyata,T. (2002) MAFFT: a novel method for rapid multiple sequence alignment based on fast Fourier transform. *Nucleic Acids Res.*, **30**, 3059–3066.

44. Clamp,M., Cuff,J., Searle,S.M. and Barton,G.J. (2004) The Jalview Java alignment editor. *Bioinformatics*, **20**, 426–427.

45. Ishihama,Y., Rappsilber,J. and Mann,M. (2006) Modular stop and go extraction tips with stacked disks for parallel and multidimensional Peptide fractionation in proteomics. *J. Proteome. Res.*, **5**, 988–994.

46. Kelstrup,C.D., Jersie-Christensen,R.R., Batth,T.S., Arrey,T.N., Kuehn,A., Kellmann,M. and Olsen,J.V. (2014) Rapid and deep proteomes by faster sequencing on a benchtop quadrupole ultra-high-field Orbitrap mass spectrometer. *J. Proteome. Res.*, **13**, 6187–6195.

47. Cox,J., Hein,M.Y., Luber,C.A., Paron,I., Nagaraj,N. and Mann,M. (2014) Accurate proteome-wide label-free quantification by delayed normalization and maximal peptide ratio extraction, termed MaxLFQ. *Mol. Cell Proteomics.*, **13**, 2513–2526.

48. Cox,J. and Mann,M. (2008) MaxQuant enables high peptide identification rates, individualized p.p.b.-range mass accuracies and proteome-wide protein quantification. *Nat. Biotechnol.*, **26**, 1367–1372.

49. Andersen,T.E., Porse,B.T. and Kirpekar,F. (2004) A novel partial modification at C2501 in Escherichia coli 23S ribosomal RNA. *RNA*, **10**, 907–913.

50. Douthwaite,S. and Kirpekar,F. (2007) Identifying modifications in RNA by MALDI mass spectrometry. *Methods Enzymol.*, **425**, 3–20.

51. Mengel-Jorgensen,J. and Kirpekar,F. (2002) Detection of pseudouridine and other modifications in tRNA by cyanoethylation and MALDI mass spectrometry. *Nucleic Acids Res.*, **30**, e135.

52. Rappsilber,J., Mann,M. and Ishihama,Y. (2007) Protocol for micro-purification, enrichment, pre-fractionation and storage of peptides for proteomics using StageTips. *Nat. Protoc.*, **2**, 1896–1906.

53. Boersema,P.J., Raijmakers,R., Lemeer,S., Mohammed,S. and Heck,A.J. (2009) Multiplex peptide stable isotope dimethyl labeling for quantitative proteomics. *Nat. Protoc.*, **4**, 484–494.

54. Edupuganti,R.R., Geiger,S., Lindeboom,R.G.H., Shi,H., Hsu,P.J., Lu,Z., Wang,S.Y., Baltissen,M.P.A., Jansen,P.W.T.C., Rossa,M. *et al.* (2017) N(6)-methyladenosine (m(6)A) recruits and repels proteins to regulate mRNA homeostasis. *Nat. Struct. Mol. Biol.*, **24**, 870–878.

55. Ingolia,N.T., Brar,G.A., Rouskin,S., McGeachy,A.M. and Weissman,J.S. (2012) The ribosome profiling strategy for monitoring translation in vivo by deep sequencing of ribosome-protected mRNA fragments. *Nat. Protoc.*, **7**, 1534–1550.

56. Lecanda,A., Nilges,B.S., Sharma,P., Nedialkova,D.D., Schwarz,J., Vaquerizas,J.M. and Leidel,S.A. (2016) Dual randomization of oligonucleotides to reduce the bias in ribosome-profiling libraries. *Methods*, **107**, 89–97.

57. Nedialkova,D.D. and Leidel,S.A. (2015) Optimization of codon translation rates via tRNA modifications maintains proteome integrity. *Cell*, **161**, 1606–1618.

58. Love,M.I., Huber,W. and Anders,S. (2014) Moderated estimation of fold change and dispersion for RNA-seq data with DESeq2. *Genome Biol.*, **15**, 550.

59. Eden,E., Navon,R., Steinfeld,I., Lipson,D. and Yakhini,Z. (2009) GOrilla: a tool for discovery and visualization of enriched GO terms in ranked gene lists. *BMC. Bioinformatics.*, **10**, 48.

60. Bheemanaik,S., Reddy,Y.V. and Rao,D.N. (2006) Structure, function and mechanism of exocyclic DNA methyltransferases. *Biochem. J.*, **399**, 177–190.

61. Timinskas,A., Butkus,V. and Janulaitis,A. (1995) Sequence motifs characteristic for DNA [cytosine-N4] and DNA [adenine-N6] methyltransferases. Classification of all DNA methyltransferases. *Gene*, **157**, 3–11.

62. Hamey,J.J., Winter,D.L., Yagoub,D., Overall,C.M., Hart-Smith,G. and Wilkins,M.R. (2015) Novel N-terminal and lysine methyltransferases that target translation elongation factor 1A in yeast and human. *Mol. Cell Proteomics.*, **15**, 164–176.

63. Sheng,Y., Laister,R.C., Lemak,A., Wu,B., Tai,E., Duan,S., Lukin,J., Sunnerhagen,M., Srisailam,S., Karra,M. *et al.* (2008) Molecular basis of Pirh2-mediated p53 ubiquitylation. *Nat. Struct. Mol. Biol.*, **15**, 1334–1342.

64. Greaves,J. and Chamberlain,L.H. (2011) DHHC palmitoyl transferases: substrate interactions and (patho)physiology. *Trends Biochem. Sci.*, **36**, 245–253.

65. Rana,M.S., Kumar,P., Lee,C.J., Verardi,R., Rajashankar,K.R. and Banerjee,A. (2018) Fatty acyl recognition and transfer by an integral membrane S-acyltransferase. *Science*, **359**, eaao6326.

66. Sekiguchi,T., Hayano,T., Yanagida,M., Takahashi,N. and Nishimoto,T. (2006) NOP132 is required for proper nucleolus localization of DEAD-box RNA helicase DDX47. *Nucleic. Acids Res.*, **34**, 4593–4608.

67. Harcourt,E.M., Ehrenschwender,T., Batista,P.J., Chang,H.Y. and Kool,E.T. (2013) Identification of a selective polymerase enables detection of N(6)-methyladenosine in RNA. *J Am. Chem. Soc.*, **135**, 19079–19082.

68. Linder,B., Grozhik,A.V., Olarerin-George,A.O., Meydan,C., Mason,C.E. and Jaffrey,S.R. (2015) Single-nucleotide-resolution mapping of m6A and m6Am throughout the transcriptome. *Nat. Methods*, **12**, 767–772.

69. Wang,S., Wang,J., Zhang,X., Fu,B., Song,Y., Ma,P., Gu,K., Zhou,X., Zhang,X., Tian,T. *et al.* (2016) N(6)-Methyladenine hinders RNA- and DNA-directed DNA synthesis: application in human rRNA methylation analysis of clinical specimens. *Chem. Sci.*, **7**, 1440–1446.

70. Sharma,S., Marchand,V., Motorin,Y. and Lafontaine,D.L.J. (2017) Identification of sites of 2′-O-methylation vulnerability in human ribosomal RNAs by systematic mapping. *Sci. Rep.*, **7**, 11490.

71. van Tran,N., Ernst,F.G.M., Hawley,B.R., Zorbas,C., Ulryck,N., Hackert,P., Bohnsack,K.E., Bohnsack,M.T., Jaffrey,S.R., Graille,M. *et al.* (2019) The human 18S rRNA m6A methyltransferase METTL5 is stabilized by TRMT112. *Nucleic Acids Res.*, **47**, 7719–7733.

72. Ma,H., Wang,X., Cai,J., Dai,Q., Natchiar,S.K., Lv,R., Chen,K., Lu,Z., Chen,H., Shi,Y.G. *et al.* (2019) N(6-)Methyladenosine methyltransferase ZCCHC4 mediates ribosomal RNA methylation. *Nat. Chem. Biol.*, **15**, 88–94.

73. Yu,Y.T. and Meier,U.T. (2014) RNA-guided isomerization of uridine to pseudouridine–pseudouridylation. *RNA. Biol.*, **11**, 1483–1494.

74. Darzacq,X., Kittur,N., Roy,S., Shav-Tal,Y., Singer,R.H. and Meier,U.T. (2006) Stepwise RNP assembly at the site of H/ACA RNA transcription in human cells. *J. Cell Biol.*, **173**, 207–218.

75. Kukalev,A.S., Lobov,I.B., Percipalle,P. and Podgornaya,O.I. (2009) SAF-A/hnRNP-U localization in interphase and metaphase. *Cytogenet. Genome Res.*, **124**, 288–297.

76. Ingolia,N.T., Ghaemmaghami,S., Newman,J.R. and Weissman,J.S. (2009) Genome-wide analysis in vivo of translation with nucleotide resolution using ribosome profiling. *Science*, **324**, 218–223.

77. Presnyak,V., Alhusaini,N., Chen,Y.H., Martin,S., Morris,N., Kline,N., Olson,S., Weinberg,D., Baker,K.E., Graveley,B.R. *et al.* (2015) Codon optimality is a major determinant of mRNA stability. *Cell*, **160**, 1111–1124.

78. Jakobsson,M.E., Malecki,J., Nilges,B.S., Moen,A., Leidel,S.A. and Falnes,P.O. (2017) Methylation of human eukaryotic elongation factor alpha (eEF1A) by a member of a novel protein lysine methyltransferase family modulates mRNA translation. *Nucleic Acids Res.*, **45**, 8239–8254.

79. Grosjean,H. and Westhof,E. (2016) An integrated, structure- and energy-based view of the genetic code. *Nucleic Acids Res.*, **44**, 8020–8040.

80. Hanson,G. and Coller,J. (2018) Codon optimality, bias and usage in translation and mRNA decay. *Nat. Rev. Mol. Cell Biol.*, **19**, 20–30.

81. Gazin,C., Wajapeyee,N., Gobeil,S., Virbasius,C.M. and Green,M.R. (2007) An elaborate pathway required for Ras-mediated epigenetic silencing. *Nature*, **449**, 1073–1077.

82. Wajapeyee,N., Malonia,S.K., Palakurthy,R.K. and Green,M.R. (2013) Oncogenic RAS directs silencing of tumor suppressor genes through ordered recruitment of transcriptional repressors. *Genes Dev.*, **27**, 2221–2226.

83. Andersen,K.R., Leksa,N.C. and Schwartz,T.U. (2013) Optimized E. coli expression strain LOBSTR eliminates common contaminants from His-tag purification. *Proteins*, **81**, 1857–1861.